



1 **Chemical cycling and deposition of atmospheric mercury**
2 **in Polar Regions: review of recent measurements and**
3 **comparison with models**

4

5 **Hélène Angot¹, Ashu Dastoor², Francesco De Simone³, Katarina Gårdfeldt⁴,**
6 **Christian N. Gencarelli³, Ian M. Hedgecock³, Sarka Langer⁵, Olivier Magand^{6, 1},**
7 **Michelle N. Mastromonaco⁴, Claus Nordstrøm⁷, Katrine A. Pfaffhuber⁸, Nicola**
8 **Pirrone⁹, Andrei Ryjkov², Noelle E. Selin^{10, 11}, Henrik Skov⁷, Shaojie Song¹⁰,**
9 **Francesca Sprovieri³, Alexandra Steffen¹², Kenjiro Toyota¹², Oleg Travnikov¹³,**
10 **Xin Yang¹⁴, Aurélien Dommergue^{1, 6}**

11 ¹Univ. Grenoble Alpes, Laboratoire de Glaciologie et Géophysique de l'Environnement
12 (LGGE), 38041 Grenoble, France

13 ²Air Quality Research Division, Environment and Climate Change Canada, 2121
14 TransCanada Highway, Dorval, Quebec H9P 1J3, Canada

15 ³CNR-Institute of Atmospheric Pollution Research, Division of Rende, UNICAL-
16 Polifunzionale, 87036 Rende, Italy

17 ⁴Department of Chemistry and Chemical Engineering, Chalmers University of Technology
18 SE-412 96 Göteborg, Sweden

19 ⁵IVL Swedish Environmental Research Institute, P.O. Box 530 21, 400 14 Göteborg, Sweden

20 ⁶CNRS, Laboratoire de Glaciologie et Géophysique de l'Environnement (LGGE), 38041
21 Grenoble, France

22 ⁷National Environmental Research Institute, Frederiksborgvej 399, 4000 Roskilde, Denmark

23 ⁸Norwegian Institute for Air Research (NILU), P.O. Box 100, 2027 Kjeller, Norway

24 ⁹CNR-Institute of Atmospheric Pollution Research, Area della Ricerca di Roma 1,
25 Monterotondo, 00015 Rome, Italy

26 ¹⁰Department of Earth, Atmospheric and Planetary Sciences, Massachusetts Institute of
27 Technology, Cambridge, MA, USA



28 ¹¹Institute for Data, Systems, and Society, Massachusetts Institute of Technology, Cambridge,
29 MA, USA

30 ¹²Air Quality Research Division, Environment and Climate Change Canada, Toronto, Ontario
31 M3H 5T4, Canada

32 ¹³Meteorological Synthesizing Centre, East of EMEP, 2nd Roshchinsky proezd, 8/5, 115419
33 Moscow, Russia

34 ¹⁴British Antarctic Survey, Cambridge, United Kingdom

35 Correspondence to: A. Dommergue (aurelien.dommergue@univ-grenoble-alpes.fr)

36

37 **Abstract**

38 Mercury (Hg) is a worldwide contaminant that can cause adverse health effects to wildlife and
39 humans. While atmospheric modeling traces the link from emissions to deposition of Hg onto
40 environmental surfaces, large uncertainties arise from our incomplete understanding of
41 atmospheric processes (oxidation pathways, deposition, and reemission). Atmospheric Hg
42 reactivity is exacerbated in high latitudes and there is still much to be learned from Polar
43 Regions in terms of atmospheric processes. This paper provides a synthesis of the
44 atmospheric Hg monitoring data available in recent years (2011-2015) in the Arctic and in
45 Antarctica along with a comparison of these observations with numerical simulations using
46 four cutting-edge global models. The cycle of atmospheric Hg in the Arctic and in Antarctica
47 presents both similarities and differences. Coastal sites in the two regions are both influenced
48 by springtime atmospheric Hg depletion events and by summertime snowpack reemission and
49 oceanic evasion of Hg. The cycle of atmospheric Hg differs between the two regions
50 primarily because of their different geography. While Arctic sites are significantly influenced
51 by Northern Hemispheric Hg emissions especially in winter, coastal Antarctic sites are
52 significantly influenced by the reactivity observed on the East Antarctic ice sheet due to
53 katabatic winds. Based on the comparison of multi-model simulations with observations, this
54 paper discusses whether the processes that affect atmospheric Hg seasonality and inter-annual
55 variability are appropriately represented in the models, and identifies research gaps in our
56 understanding of the atmospheric Hg cycling in high latitudes.

57

58



59 1 Introduction

60 Mercury (Hg) can be emitted to the atmosphere by natural geological sources (e.g., volcanic
61 emissions) and a variety of anthropogenic activities (e.g., coal combustion, artisanal and
62 small-scale gold mining) (UNEP, 2013b). The dominant form of atmospheric mercury is
63 gaseous elemental mercury (Hg(0)) (Lindberg and Stratton, 1998). Hg(0) has an atmospheric
64 lifetime of 0.5 to 1 year (Selin, 2009) and can therefore be transported worldwide. It can be
65 oxidized into highly reactive and water soluble gaseous and particulate divalent species
66 (Hg(II) and Hg(p), respectively) that can deposit onto environmental surfaces (e.g., land,
67 surface oceans) through wet and dry processes (Lindqvist and Rodhe, 1985). Upon deposition,
68 mercury can be reemitted to the atmosphere or converted – in aquatic systems – to
69 methylmercury (Driscoll et al., 2013). Anthropogenic activities have altered the global
70 geochemical cycle of mercury, enhancing the amount of mercury circulating in the
71 atmosphere and surface oceans by at least a factor of three (Lamborg et al., 2014; Amos et
72 al., 2015).

73 Methylmercury is a worldwide contaminant of seafood that can cause adverse effects on the
74 developing nervous system of vulnerable populations (AMAP, 2015). The Minamata
75 Convention on mercury – global treaty to protect human health and the environment from
76 mercury – was opened for signature in October 2013 (UNEP, 2013a). To date, the Convention
77 has been signed by 128 countries and ratified by 28. It will enter into force once it is ratified
78 by 50 nations. As noted in the preamble of the Convention, Arctic ecosystems and indigenous
79 communities are particularly vulnerable due to the biomagnification of mercury and
80 contamination of traditional foods. In order to reduce mercury effects, the pathway from
81 emissions to human and environmental impacts needs to be traced. Atmospheric modeling
82 provides a first step by tracing the link from emissions to deposition onto environmental
83 surfaces. Deposition of mercury in a particular region depends on the magnitude and
84 speciation of domestic and foreign emissions, and on the oxidative capacity of the atmosphere
85 that transforms Hg(0) to deposited divalent species (UNEP, 2015). Deposition is partly offset
86 by the revolatilization of a fraction of deposited mercury. Large uncertainties associated with
87 the models arise as a result of our incomplete understanding of atmospheric processes (e.g.,
88 oxidation pathways, deposition, and reemission) (Kwon and Selin, 2016). Atmospheric
89 mercury reactivity is exacerbated in high latitudes and there is still much to be learned from
90 Polar Regions in terms of atmospheric processes.



91 First discovered in 1995 (Schroeder et al., 1998), Atmospheric Mercury Depletion Events
92 (AMDEs) are observed in springtime throughout the Arctic (Lindberg et al., 2001; Berg et
93 al., 2003a; Poissant and Pilote, 2003; Skov et al., 2004; Steffen et al., 2005) as a result of
94 the oxidation of Hg(0) by reactive bromine species (Lu et al., 2001; Brooks et al., 2006;
95 Sommar et al., 2007). AMDEs can lead to a deposition of ~ 100 tons of mercury per year to
96 the Arctic (Ariya et al., 2004; Skov et al., 2004; Dastoor et al., 2015). The fate of mercury
97 deposited onto the snowpack during AMDEs is still a matter of debate in the scientific
98 mercury community (Steffen et al., 2008). Several studies reported significant reemission
99 (e.g., Ferrari et al., 2005; Brooks et al., 2006; Kirk et al., 2006; Sommar et al., 2007;
100 Dommergue et al., 2010a) although a fraction of mercury may likely accumulate within the
101 snowpack (Hirdman et al., 2009; Larose et al., 2010). While the Arctic has been extensively
102 monitored – with hundreds of publications focusing on AMDEs, measurements are sporadic
103 in Antarctica. To the best of the author’s knowledge, only eleven studies dealing with
104 atmospheric mercury in Antarctica (and using modern instrument) have been published
105 (Ebinghaus et al., 2002; Sprovieri et al., 2002; Temme et al., 2003; Brooks et al., 2008a;
106 Brooks et al., 2008b; Dommergue et al., 2012; Pfaffhuber et al., 2012; Angot et al., 2016a;
107 Angot et al., 2016b; Nerentorp Mastromonaco et al., 2016; Wang et al., 2016). The earliest
108 studies showed the occurrence of AMDEs in coastal Antarctica after polar sunrise. The latest
109 studies highlighted new atmospheric processes in the Antarctic boundary layer – both in
110 winter and summertime – leading to the formation and subsequent deposition of reactive
111 mercury. In the meantime, several studies showed that the Antarctic Plateau plays a key role
112 in influencing the cycle of atmospheric mercury at a continental scale.

113 The first objective of this paper is to provide a synthesis of the atmospheric mercury
114 monitoring data available in recent years (2011-2015) in Polar Regions. Secondly, we provide
115 a comparison of these observations with numerical simulations of atmospheric mercury
116 concentrations using cutting-edge global models. Finally, this paper identifies research gaps in
117 our understanding and modeling of the atmospheric mercury cycling in high latitudes.

118



119 **2 Experimental Section**

120 **2.1 Measurements of atmospheric mercury species**

121 **2.1.1 Definitions**

122 Hg(0), Hg(II), and Hg(p) are the most abundant mercury species in the atmosphere.
123 Atmospheric Hg(0) is easily and accurately measured in Polar Regions (Steffen et al., 2008;
124 Dommergue et al., 2010b). Hg(p) and Reactive Gaseous Mercury (RGM) – the latter
125 consisting of various gaseous Hg(II) compounds – are operationally defined. Total Gaseous
126 Mercury (TGM) refers to the sum of Hg(0) and Hg(II), and Reactive Mercury (RM) to the
127 sum of RGM and Hg(p).

128 **2.1.2 Instrumentation**

129 Measurements of atmospheric mercury species were performed at various sites in the Arctic
130 and in Antarctica over the 2011-2015 period (Fig. 1). All Hg(0) measurements reported in this
131 paper were performed using a Tekran gas phase analyzer (Model 2537), and all RGM and
132 Hg(p) measurements using a Tekran speciation unit (1130/1135) (Table 1). The Tekran 2537
133 analyzer is based on the amalgamation of mercury onto a gold cartridge followed by a thermal
134 desorption and detection by an integrated cold vapor atomic fluorescence spectrometer
135 (CVAFS) at 253.7 nm (Fitzgerald and Gill, 1979; Bloom and Fitzgerald, 1988). The analysis
136 of Hg(0) is semi-continuous and the presence of two gold cartridges allows alternating
137 sampling and desorption modes. At all sampling sites, the sample air stream was prefiltered
138 either through a Tekran speciation unit or through a sodalime trap and/or a PTFE
139 (polytetrafluoroethylene) filter (Table 1). Some researchers report ambient air collected at
140 Polar sites as TGM (Ebinghaus et al., 2002), instead of Hg(0), but the PTFE filter on the front
141 of the analyzer inlet most likely removes RGM and thus only Hg(0) is collected and analyzed
142 (Steffen et al., 2002; Steffen et al., 2008). Due to the extremely cold and dry air in Antarctica,
143 no heated sampling line was used and no sodalime was applied at TR, DC, and DDU.
144 Collected at 5 to 15 min intervals at the various sites, Hg(0) measurements are reported here
145 as hourly averages. RGM and Hg(p) measurements at ALT and ANT were performed using a
146 Tekran speciation unit – connected to a 2537 analyzer through a PTFE heated sampling line –
147 through a multistep procedure as described elsewhere (Lindberg et al., 2002) using an
148 impactor inlet (2.5 μm cut-off aerodynamic diameter at 10 L/min), a KCl-coated quartz



149 annular denuder in the 1130 unit, and a quartz regenerable particulate filter (RPF) in the 1135
150 unit.

151 **Quality assurance and quality control procedures**

152 Auto-calibrations of the 2537 analyzers were performed every 25 to 72 hours at the various
153 sites using an internal mercury permeation source. The accuracy of this permeation source
154 was checked at least once per year against manual injections using a Tekran 2505 mercury
155 vapor calibration unit and following a strict procedure adapted from Dumarey et al. (1985).
156 The detection limit for Hg(0) measurements is 0.10 ng/m³ according to the instrument manual
157 (Tekran, 2011). Based on experimental evidence, the average systematic uncertainty for
158 Hg(0) measurements is of ~ 10 % (Slemr et al., 2015). There is no robust calibration
159 technique of the Tekran speciation unit and no certified reference material available. There is
160 growing evidence that RGM and Hg(p) might suffer from significant biases and interferences
161 (Lyman et al., 2010; Gustin et al., 2013; Jaffe et al., 2014; Huang et al., 2013; Kos et al.,
162 2013), and that RGM concentrations might be underestimated by as much as a factor of 2 - 13
163 (Gustin et al., 2016). Despite these limitations, the Tekran speciation unit is currently the best
164 available automated method, and Hg(p) and RGM measurements can be used as first
165 estimates to evaluate atmospheric models. Maintenance operations on the Tekran
166 2537/1130/1135 instruments and screening criteria for data validation/invalidation were
167 performed according to the directives of the standard operational procedure (SOP) from
168 CAMNet (Canadian Mercury Measurement Network), AMNet (United States Atmospheric
169 Mercury Network), or GMOS (Global Mercury Observation System) (Steffen et al., 2012;
170 D'Amore et al., 2015).

171 **2.2 Global mercury simulations**

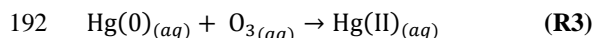
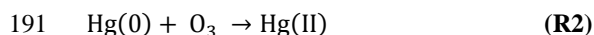
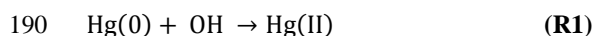
172 The current study is based on multi-model simulations performed as part of the Mercury
173 Modeling Task Force (MMTF) under the GMOS project (Travnikov et al., in preparation).
174 Four global models (ECHMERIT, GEM-MACH-Hg, GEOS-Chem, and GLEMOS) were
175 applied for evaluating monthly-averaged atmospheric mercury concentrations and deposition
176 at various Arctic and Antarctic ground-based sites for the year 2013. Additionally, GEM-
177 MACH-Hg and GEOS-Chem provided hourly-averaged data from 2011 to 2014 to allow
178 investigations of inter-annual variability. A brief description of the parameterization of the
179 four models is given below. The models differ significantly in their description of mercury



180 atmospheric chemistry and their parameterization of processes specific to Polar Regions (i.e.,
181 AMDEs, oceanic evasion, and re-emissions from the snowpack).

182 **2.2.1 ECHMERIT**

183 ECHMERIT is a fully-coupled model, based on the Atmospheric General Circulation Model
184 (AGCM) ECHAM5, and a mercury chemistry module, developed at the Institute for
185 Atmospheric Pollution of the National Research Council (CNR-IIA) of Italy (Jung et al.,
186 2009; De Simone et al., 2014; De Simone et al., 2016). The base mechanism includes
187 oxidation of Hg(0) by OH and O₃ in the gas and aqueous (in-cloud) phases (reactions R1 to
188 R3). Rate constants of reactions (R1) to (R3) are from Sommar et al. (2001), Hall (1995), and
189 Munthe (1992), respectively.



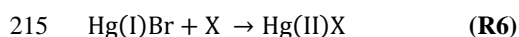
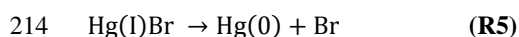
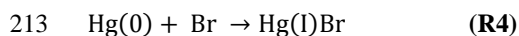
193 Oxidant fields (OH/O₃) are imported from MOZART (Model for Ozone and Related
194 Chemical Tracers) (Emmons et al., 2010). In the base run used for this work bromine
195 chemistry is not included, and there is no parameterization of AMDEs. ECHMERIT
196 implements dynamically calculated ocean emissions for all ice-free basins, including Polar
197 Regions, as described in De Simone et al. (2014), and a prompt re-emission of 60 % of
198 deposited mercury over ice (Selin et al., 2008).

199 **2.2.2 GEM-MACH-Hg**

200 GEM-MACH-Hg is a mercury version of the Environment and Climate Change Canada's
201 (ECCC's) current operational air quality forecast model – Global Environmental Multi-scale –
202 Modelling air quality and Chemistry (GEM-MACH). GEM-MACH-Hg is an on-line model,
203 meaning that the meteorology is simulated in-step with the chemistry, and includes
204 representation of physicochemical processes of mercury based on the ECCC's previous
205 mercury model – GRAHM (Dastoor and Larocque, 2004; Dastoor et al., 2008; Durnford et
206 al., 2010; Durnford et al., 2012; Kos et al., 2013; Dastoor et al., 2015). The horizontal
207 resolution of the model for this study is 1° × 1° latitude/longitude. Hg(0) is oxidized in the
208 atmosphere by OH (R1) and bromine (reactions (R4) to (R6), X = Br or BrO). The rate
209 constant of (R1) is from Sommar et al. (2001), but scaled down by a coefficient of 0.34 to
210 take into account possible dissociation reactions (Tossell, 2003; Goodsite et al., 2004). Rate



211 constants of reactions (R4) to (R6) are from Donohoue et al. (2006), Dibble et al. (2012) and
 212 Goodsite et al. (2004), respectively. Aqueous-phase reduction reactions are not included.



216 OH fields are from MOZART (Emmons et al., 2010) while BrO is derived from 2007-2009
 217 satellite observations of BrO vertical columns. The associated Br concentration is then
 218 calculated from photochemical steady state according to equation (1), where J_{BrO} is the BrO
 219 photolysis frequency, and $k_1 = 2.1 \cdot 10^{-11} \text{ cm}^3 \text{ molecule}^{-1} \text{ s}^{-1}$ and $k_2 = 1.2 \cdot 10^{-12} \text{ cm}^3 \text{ molecule}^{-1} \text{ s}^{-1}$
 220 ¹ are the rate coefficients for the $\text{BrO} + \text{NO} \rightarrow \text{Br} + \text{NO}_2$ and $\text{Br} + \text{O}_3 \rightarrow \text{BrO} + \text{O}_2$
 221 reactions, respectively (Platt and Janssen, 1995).

$$222 \quad \frac{[\text{Br}]}{[\text{BrO}]} = \frac{J_{\text{BrO}} + k_1 [\text{NO}]}{k_2 [\text{O}_3]} \quad (1)$$

223 Durnford et al. (2012) developed and implemented a dynamic multilayer snowpack/meltwater
 224 parameterization allowing the representation of deposition and reemission of mercury.
 225 Oceanic evasion of Hg(0) is activated if there is open water and the temperature at the air-sea
 226 interface is $-4 \text{ }^\circ\text{C}$ or greater (Dastoor and Durnford, 2014). In addition, Hg(0) released from
 227 sea ice melting is also taken into account. The parameterization of AMDEs is based on Br
 228 production and chemistry, and snow reemission of Hg(0) (Dastoor et al., 2008).

229 **2.2.3 GEOS-Chem**

230 GEOS-Chem (v9-02) is a global chemical transport model driven by assimilated
 231 meteorological data from the NASA GMAO Goddard Earth Observing System (Bey et al.,
 232 2001). It couples a 3-D atmosphere (Holmes et al., 2010), a 2-D mixed layer slab ocean
 233 (Soerensen et al., 2010), and a 2-D terrestrial reservoir (Selin et al., 2008) with a horizontal
 234 resolution of $2^\circ \times 2.5^\circ$ latitude/longitude. Three mercury tracers (Hg(0), Hg(II), and Hg(p))
 235 are tracked in the atmosphere (Amos et al., 2012). Mercury fluxes at terrestrial and ocean
 236 surfaces are described in Song et al. (2015). A two-step oxidation mechanism initialized by Br
 237 atoms is used (reactions (R4) to (R6), $\text{X} = \text{Br}$ or OH). Br fields are archived from a full-
 238 chemistry GEOS-Chem simulation (Parrella et al., 2012) while rate constants of reactions
 239 (R4) to (R6) are from Donohoue et al. (2006), Balabanov et al. (2005), and Goodsite et al.
 240 (2012), respectively. Some model setups related to Polar Regions are implemented in v9-02 of



241 the model as described in details in Holmes et al. (2010). 5 pptv of BrO – at the low end of
242 concentrations reported by Neuman et al. (2010) – is added in the springtime Arctic
243 (Antarctic) boundary layer during March-May (August-October) over areas with sea ice,
244 sunlight, stable conditions, and temperatures below 268 K. The associated Br concentration is
245 then calculated from photochemical steady state according to equation (1) assuming that O₃ is
246 depleted to 2 ppbv. Additionally, a snowpack reservoir is added. It accumulates deposited
247 mercury and releases it as Hg(0) under sunlit conditions in a temperature-dependent way.

248 2.2.4 GLEMOS

249 GLEMOS (Global EMEP Multi-media Modelling System) is a multi-scale chemical transport
250 model developed for the simulation of environmental dispersion and cycling of different
251 chemicals including mercury (Travnikov and Ilyin, 2009). The model simulates atmospheric
252 transport, chemical transformations and deposition of three mercury species (Hg(0), Hg(II),
253 and Hg(p)). The atmospheric transport of tracers is driven by meteorological fields generated
254 by the Weather Research and Forecast (WRF) modelling system (Skamarock et al., 2007) fed
255 by the operational analysis data from ECMWF. The model in the base configuration has a
256 horizontal resolution of 1° × 1°. The base mechanism includes oxidation of Hg(0) by OH
257 (R1) and O₃ (R2) in the atmosphere. Rate constants are from Sommar et al. (2001) and Hall
258 (1995), respectively. The model also includes in-cloud oxidation of Hg(0) by OH, O₃, and Cl
259 with associated rate constants from Gårdfeldt et al. (2001), Munthe (1992), and Lin and
260 Pehkonen (1999), respectively. In-cloud reduction by SO₃²⁻ is also implemented, with an
261 associated rate constant from Petersen et al. (1998). Reactant fields are imported from
262 MOZART (Emmons et al., 2010).

263 The parameterization of AMDEs in Polar Regions is based on Br chemistry following the
264 two-step mechanism (R4)-(R6) described in Holmes et al. (2010). Br concentrations are
265 extracted from p-TOMCAT (parallel-Tropospheric Off-Line Model of Chemistry and
266 Transport) results (Yang et al., 2005). GLEMOS includes an empirical parameterization of
267 prompt-reemission from snow. It is assumed that reemission occurs only from newly
268 deposited mercury in the presence of solar radiation. Two competing processes are
269 considered: photoreduction and ageing of deposited mercury with the characteristic times of 1
270 day and 10 days, respectively. It is also assumed that all reduced mercury is immediately
271 reemitted back to the atmosphere. The aged fraction of mercury does not undergo reduction
272 and is accumulated within the snowpack. No mercury evasion from the ocean is implemented.



273 **2.3 Goodness-of-fit statistics between modeled and observed data**

274 The Nash-Sutcliffe efficiency (NSE, Nash and Sutcliffe, 1970) indicates how well the plot of
275 observed versus simulated data fits the 1:1 line – NSE = 1 corresponding to the perfect match.
276 NSE is defined as one minus the sum of the absolute squared differences between the
277 simulated and observed values normalized by the variance of the observed values:

$$278 \quad \text{NSE} = 1 - \frac{\sum_{i=1}^N (O_i - S_i)^2}{\sum_{i=1}^N (O_i - \bar{O})^2} \quad (2)$$

279 The root mean square error (RMSE) gives the standard deviation of the model prediction error
280 (in the same units of simulated and observed values). A smaller value indicates better model
281 performance. It is calculated as follows:

$$282 \quad \text{RMSE} = \sqrt{\frac{1}{N} \sum_{i=1}^N (S_i - O_i)^2} \quad (3)$$

283 The percent bias (PBIAS, in %) measures the average tendency of the simulated values to be
284 larger or smaller than their observed ones. The optimal value of PBIAS is 0. PBIAS is
285 calculated as follows:

$$286 \quad \text{PBIAS} = 100 \frac{\sum_{i=1}^N (S_i - O_i)}{\sum_{i=1}^N O_i} \quad (4)$$

287 NSE, RMSE, and PBIAS were calculated by using the R package “hydroGOF” (Zambrano-
288 Bigiarini, 2014).

289

290 **3 Results and Discussion**

291 **3.1 Arctic sites**

292 **3.1.1 Observations**

293 Fig. 2a shows monthly box plots of all data collected at the four Arctic sites. The average
294 Hg(0) value in the Arctic over the 2011-2014 period is $1.46 \pm 0.33 \text{ ng m}^{-3}$. This concentration
295 falls within the range of what is observed in the Northern Hemisphere (Sprovieri et al., this
296 issue-a). The highest mean is at AND ($1.55 \pm 0.15 \text{ ng m}^{-3}$ over the 2011-2015 period), which
297 is closer from European industrialized areas than other sites and experiences less frequent and
298 pronounced AMDEs in spring (see section 3.1.1.2). There is a clear Hg(0) concentration
299 gradient (except from June to August): AND > NYA > SND > ALT.



300 The Hg(0) concentration data from the four Arctic sites for the period 2011-2015 are
301 presented as monthly box and whisker plots in Fig. 3. Information regarding annually- and
302 monthly-based statistics at the three sites can be found in Tables 2 and 3, respectively. The
303 annual medians at NYA and AND (Table 2) suggest a low inter annual variability in the
304 distribution of Hg(0) concentrations. Conversely, there is a high degree of inter-annual
305 variability at ALT and SND driven by the intensity of spring and summertime processes. This
306 will be addressed in the following sections.

307 The mean seasonal variation of Hg(0) concentrations at Arctic sites is displayed in Fig. 4a.
308 Summer refers to June – August, fall to September – November, winter to December –
309 February, and spring to March – May. Hg(0) concentrations exhibit a strong and consistent
310 seasonal pattern year after year, as already reported by others (Steffen et al., 2005; Berg et
311 al., 2013). Hg(0) concentrations reach a distinct maximum in summer at ALT, SND, and
312 NYA (mean concentrations of 1.63 ± 0.37 , 1.63 ± 0.37 , and 1.60 ± 0.23 ng m⁻³, respectively).
313 In late summer the concentrations start to decrease and reach in fall a mean value of $1.28 \pm$
314 0.12 ng m⁻³ at ALT, 1.36 ± 0.11 ng m⁻³ at SND, and 1.46 ± 0.16 ng m⁻³ at NYA. In winter,
315 concentrations increase slightly and are significantly higher than in fall at the three sites (*p*
316 value < 0.0001 at the three sites, Mann-Whitney test). Springtime reflects the lowest Hg(0)
317 concentrations with mean values of 1.11 ± 0.58 ng m⁻³ at ALT, 1.28 ± 0.51 ng m⁻³ at SND,
318 and 1.38 ± 0.38 ng m⁻³ at NYA. The seasonal cycle is more pronounced at ALT than at SND
319 and NYA. Hg(0) concentrations at AND exhibit an opposite seasonal cycle with a
320 significantly (*p* value < 0.0001, Mann-Whitney test) higher mean concentration in winter
321 (1.67 ± 0.11 ng m⁻³) than in summer (1.48 ± 0.12 ng m⁻³), in line with the seasonality reported
322 at Pallas, Finland (67°22'N, 26°39'E) (Berg et al., 2001; Sprovieri et al., this issue-a). The
323 mechanisms which cause the seasonal variation of Hg(0) concentrations at Arctic sites are
324 discussed in the following sections.

325 **3.1.1.1 Wintertime advection of Hg from mid-latitudes**

326 Several studies highlighted that the Arctic is significantly influenced by atmospheric pollution
327 from mid-latitudes – phenomenon known as Arctic haze – during wintertime (Barrie et al.,
328 1981; Heintzenberg et al., 1981; Shaw, 1982; Heidam et al., 1999; Heidam et al., 2004;
329 Bourgeois and Bey, 2011; Nguyen et al., 2013). Dastoor and Larocque (2004) used an on-line
330 model to explain the observed seasonal variations in atmospheric mercury circulation and
331 showed frequent episodes of mercury transport from mid-latitudes sources to the Arctic in
332 winter. Similarly, Hirdman et al. (2009) attributed the highest 10 % of all wintertime Hg(0)



333 data at NYA to transport of air masses especially from Europe. Higher Hg(0) concentrations
334 in winter compared to fall at ALT, SND, and NYA can therefore be attributed to the
335 meteorological differences in the seasonal circulation patterns (Dastoor and Larocque, 2004).
336 Higher concentrations in winter at AND compared to the three other Arctic sites can be
337 attributed to the powerful advection of air masses from Europe at this site (Durnford et al.,
338 2010).

339 3.1.1.2 Springtime AMDEs

340 AMDEs in the Arctic are defined as Hg(0) concentrations below 1.00 ng m^{-3} (Steffen et al.,
341 2005; Cobbett et al., 2007). Based on this threshold, AMDEs occur in 39 %, 28%, 15%, and
342 1% of the 2011-2014 springtime observations at ALT, SND, NYA, and AND, respectively.
343 The fact that ALT experiences stronger and more frequent AMDEs than other Arctic sites
344 could be due to air masses circulation patterns. Several studies indicated that a large fraction
345 of the AMDEs reported at NYA and AND are suspected to result from the long-range
346 transport of air masses containing depleted Hg(0) from areas over the Arctic Ocean (Gauchard
347 et al., 2005; Sommar et al., 2007; Berg et al., 2008; Steen et al., 2011; Berg et al., 2013). A
348 statistical analysis on the results from a Lagrangian particle dispersion model (FLEXPART)
349 and Hg(0) concentrations measured at NYA was performed by Hirdman et al. (2009) to
350 identify source regions of high- and low-Hg air masses. The authors concluded that the lowest
351 10% of the Hg(0) data at NYA in spring were strongly associated with transport across the
352 sea-ice covered Arctic Ocean at low altitudes – areas where elevated BrO concentrations are
353 seen in the atmospheric column by satellite observations (e.g., Lindberg et al., 2002).
354 Similarly, a correlation of AMDEs with wind direction at ALT supports the origin of
355 depletion events over the Arctic Ocean (Cole and Steffen, 2010). The less frequent and
356 pronounced AMDEs at AND may be explained by the fact that this site is farther away from
357 the source areas of AMDEs (Berg et al., 2008).

358 Over the 2011-2015 period, AMDEs at NYA are evenly distributed between April and May as
359 38 and 38% respectively, and fewer in March and June (14 and 10 % of the time,
360 respectively). This result is in good agreement with the distribution reported by Berg et al.
361 (2013) over the 2000-2009 period. Conversely, AMDEs are more frequent in April (41 %)
362 than in May (32 %) at ALT, while less frequent in April (34 %) than in May (43 %) at SND.
363 Interestingly, the analysis of the ALT dataset from 1995 to 2007 by Cole and Steffen (2010)
364 revealed that, over time, the month of maximum AMDE activity shifted from May to April.
365 On the contrary, the analysis of the NYA dataset from 2000 to 2009 by Berg et al. (2013) did



366 not evidence such a change in the timing frequency of AMDEs. The reason for this shift in
367 timing of AMDEs at ALT is not fully understood but could be due to local meteorology (Cole
368 and Steffen, 2010). The authors found that the length, magnitude, and frequency of AMDEs
369 decreased with increasing local temperature. These results are consistent with earlier studies
370 on the temperature dependence of the halogen chemistry initiating AMDEs and ozone
371 depletion events (Koop et al., 2000; Adams et al., 2002; Tarasick and Bottenheim, 2002;
372 Sander et al., 2006) and with a modeling study reporting that increasing surface air
373 temperature decreases the frequency of AMDEs (Chen et al., 2015). However, considering
374 the fact that AMDEs observed at Arctic sites often result from the transport of depleted air
375 masses, local temperature might not be the key explanatory parameter. Moore et al. (2014)
376 showed that AMDEs and ozone depletion events near Barrow, Alaska, are directly linked to
377 sea-ice dynamics. According to the authors, depletion events are favored by consolidated sea-
378 ice cover but both Hg(0) and O₃ concentrations immediately recover to near-background
379 concentrations when air masses cross open leads within a day before measurements. The
380 authors attributed this recovery of concentrations to changes in boundary-layer dynamics
381 induced by sea-ice leads, causing significant convective mixing with non-depleted air masses
382 aloft. Further work is needed to establish the degree to which sea-ice dynamics across the
383 Arctic might influence the inter-annual variability of AMDEs at the various Arctic sites.
384 Indeed, AMDEs occurred at ALT in 36 % (2011), 51 % (2012), 50 % (2013), and 21 %
385 (2014) of the springtime observations, at SND in 37 % (2011), 16 % (2012), 36 % (2013), and
386 19 % (2014) of the springtime observations, and finally at NYA in 18 % (2011), 13 % (2012),
387 16 % (2013), 20 % (2014), and 6 % (2015) of the springtime observations.

388 Several studies reported RGM and Hg(p) concentrations during AMDEs at Arctic sites
389 (Lindberg et al., 2002; Berg et al., 2003a; Steffen et al., 2003; Aspö et al., 2005;
390 Gauchard et al., 2005; Sprovieri et al., 2005a; Steen et al., 2011; Wang, 2015). Fig. 5 shows
391 box plots of the monthly concentrations of RGM and Hg(p) at ALT over the 2011-2014
392 period. A distinct annual cycle is highlighted in this figure. Hg(p) concentrations increase
393 from November through February likely due to the Arctic haze (Steffen et al., 2014), reach a
394 maximum in March and April due to AMDEs, and then decrease. RGM concentrations peak
395 in spring and then gradually decrease. The production of RGM in June and July – after the
396 AMDEs season – is observed every year and remains unexplained (Steffen et al., 2014).
397 While Hg(p) is the dominant species in early spring, a clear shift is observed, from the
398 predominance of Hg(p) to RGM in AMDEs occurring toward the end of spring. This shift has



399 already been evidenced at Churchill, Manitoba (Kirk et al., 2006), ALT (Cobbett et al., 2007),
400 and NYA (Steen et al., 2011), and has been shown to repeat year after year at ALT (Steffen et
401 al., 2014). Steffen et al. (2014) suggested that this shift is due to temperature and particle
402 availability. Using a detailed air-snowpack model for interactions of bromine, ozone and
403 mercury in the springtime Arctic, Toyota et al. (2014) proposed that Hg(p) is mainly produced
404 as HgBr_4^{2-} through uptake of RGM into bromine-enriched aerosols after ozone is significantly
405 depleted in the air mass. In addition, Toyota et al. (2014) provided the temperature
406 dependence of these reactions which needs to be verified experimentally. Based on ten years
407 of data, Steffen et al. (2014) also reported higher levels of mercury in the snow when the
408 atmospheric conditions favored the formation of RGM. This springtime shift from the
409 predominance of Hg(p) to RGM in AMDEs likely directly impacts the amount of mercury
410 deposited onto the snowpack. This will be further discussed in section 3.1.2.2.

411 3.1.1.3 Summer enhancement of Hg(0) concentrations

412 According to Dastoor and Larocque (2004), advection of mercury from mid-latitudes to the
413 Arctic is insignificant in summer due to weak airflow movements and to a confined polar
414 front. The increase of Hg(0) concentrations in summer could be due to the reemission of
415 mercury deposited during springtime AMDEs. However, the comparison of the magnitude of
416 the springtime depletion and the magnitude of the summer enhancement at ALT suggests
417 otherwise. Mean springtime Hg(0) concentrations are lower – suggesting more intense and/or
418 frequent AMDEs – in 2012 ($0.97 \pm 0.53 \text{ ng m}^{-3}$) and 2013 ($0.89 \pm 0.57 \text{ ng m}^{-3}$) than in 2011
419 ($1.19 \pm 0.59 \text{ ng m}^{-3}$) and 2014 ($1.37 \pm 0.50 \text{ ng m}^{-3}$), while mean summertime concentrations
420 are higher – suggesting more reemission – in 2011 ($1.81 \pm 0.37 \text{ ng m}^{-3}$) and 2014 (1.63 ± 0.31
421 ng m^{-3}) than in 2012 ($1.43 \pm 0.27 \text{ ng m}^{-3}$) and 2013 ($1.65 \pm 0.41 \text{ ng m}^{-3}$). Therefore, the
422 summer enhancement of Hg(0) concentrations is generally attributed to emissions from snow
423 and ice surfaces (Poulain et al., 2004; Sprovieri et al., 2005b; Sprovieri et al., 2005a;
424 Sprovieri et al., 2010; Douglas et al., 2012) and/or to evasion from the ice-free surface waters
425 of the Arctic Ocean (Aspmo et al., 2006; Andersson et al., 2008; Hirdman et al., 2009;
426 Fisher et al., 2013; Dastoor and Durnford, 2014; Yu et al., 2014; Soerensen et al., 2016).
427 The atmospheric mercury model (GRAHM) used by Dastoor and Durnford (2014) simulated
428 a first peak in Hg(0) concentrations driven by revolatilization from snowpack/meltwaters,
429 followed by a second peak driven by oceanic evasion – the timing of the peaks varying with
430 location and year. Additional modeling studies suggested that some of the mercury in surface
431 ocean waters may come from riverine input (Fisher et al., 2012; Soerensen et al., 2016).



432 As can be seen in Fig. 3, Hg(0) concentrations are significantly higher (p value < 0.0001 ,
433 Mann-Whitney test) during summer 2011 at ALT ($1.81 \pm 0.37 \text{ ng m}^{-3}$) than during the
434 following summers ($1.57 \pm 0.35 \text{ ng m}^{-3}$ in average). At SND, Hg(0) concentrations peak in
435 summer 2013 ($1.91 \pm 0.37 \text{ ng m}^{-3}$ vs. $1.52 \pm 0.26 \text{ ng m}^{-3}$ in average during summers 2011,
436 2012, and 2014). One possible explanation for this inter-annual variability is sea ice extent.
437 Daily sea ice maps can be obtained from [http://www.iup.uni-](http://www.iup.uni-bremen.de/iuppage/psa/2001/amsrop.html)
438 [bremen.de/iuppage/psa/2001/amsrop.html](http://www.iup.uni-bremen.de/iuppage/psa/2001/amsrop.html) (Spren et al., 2008). ALT and SND are both
439 surrounded by multi-year ice. During summer 2011, the Hall Basin – waterway between
440 Greenland and Canada’s northernmost island where ALT is located – was ice-free. During
441 summer 2013, sea ice extent was particularly low in the Greenland Sea – between Greenland
442 and the Svalbard archipelago. These large areas of ice-free surface waters might have led to
443 enhanced oceanic evasion near ALT, and SND in 2011 and 2013, respectively. Indeed, Yu et
444 al. (2014) reported a negative correlation between TGM and salinity over an Arctic ice-
445 covered region, suggesting that ice melting would enhance TGM concentrations. This
446 hypothesis is further supported by wind data obtainable from
447 http://climate.weather.gc.ca/historical_data/search_historic_data_e.html and
448 <http://villumresearchstation.dk/data/>. At ALT, the summertime dominant wind direction is
449 from north-east but with frequent and strong winds from south/south-west (Hall Basin), in
450 line with results reported by Bilello (1973) and Cobbett et al. (2007). At SND, the dominant
451 wind direction is from south-west but the direction becomes more variable in summer with
452 winds also occurring from south and east (Bilello, 1973; Nguyen et al., 2013). Yet a
453 comprehensive and systematic analysis of air masses back-trajectories and sea-ice extent is
454 required to further investigate parameters responsible for the observed inter-annual variability.

455 NYA is normally surrounded by open water in the summer. Therefore, oceanic emissions are
456 expected to act as a significant local source to NYA, while being a regional and diffuse source
457 at ALT and SND (Cole et al., 2013). However, the summer enhancement of Hg(0)
458 concentrations is weaker at NYA than at ALT and SND (Fig. 4a). The western coast of
459 Spitsbergen island, where NYA is located, was ice-free year-round over the period of interest
460 possibly preventing the build-up of mercury-enriched ice-covered surface waters in winter
461 and intense evasion in summer. Additionally, a comparative study was carried out at NYA
462 with measurements at both 12 m a.s.l. and 474 m a.s.l.. While Aspino et al. (2005) found no
463 significant difference between Hg(0) concentrations at the two elevations, several studies
464 (Berg et al., 2003b; Sprovieri et al., 2005b; Sommar et al., 2007) reported that Hg(0)



465 concentrations at 12 m a.s.l. were higher in magnitude and exhibited a higher variability than
466 at 474 m a.s.l.. Evidence of volatile mercury evasion from snow and water surfaces was also
467 obtained, suggesting a cycling of mercury near the surface. Zeppelin station at 474 m a.s.l. is
468 typically positioned over or at the top of the marine boundary layer of the fjord valley
469 (Sommar et al., 2007) likely, at least partly, explaining why the summer enhancement of
470 Hg(0) concentrations is weaker at NYA.

471 In contrast to observations at ALT, SND, and NYA, Hg(0) concentrations reach a minimum
472 in summer at AND. Transport of air masses from Europe is dominant at AND (Durnford et
473 al., 2010) and could mask any variability induced by oceanic evasion. The mean Hg(0)
474 concentration in summer at AND ($1.48 \pm 0.12 \text{ ng m}^{-3}$ over the 2011-2015 period) is consistent
475 with the value of $\sim 1.42 \text{ ng m}^{-3}$ reported at Pallas, Finland over the 2013-2014 period
476 (Sprovieri et al., this issue-a).

477 **3.1.2 Comparison with models**

478 Table 4 displays goodness-of-fit statistics between monthly-averaged modeled and observed
479 data in 2013. Except at ALT, modeled Hg(0) concentrations are biased-low suggesting that
480 the four global models tend to underestimate sources of Hg(0). The ability of the four models
481 to reproduce the observed seasonality of Hg(0) concentrations at Arctic sites in 2013 is shown
482 in Fig. 6a and discussed in the following sections. As mentioned in section 2.2, GEM-MACH-
483 Hg and GEOS-Chem provided hourly-averaged data from 2011 to 2014. The inter-annual
484 variability of the monthly Hg(0) concentration distribution at Arctic sites as simulated by the
485 two models is displayed in Fig. 7a while Table 5 shows the percent bias between hourly-
486 averaged modeled and observed data on a seasonal basis from 2011 to 2014.

487 **3.1.2.1 Seasonal variation**

488 **a) Winter**

489 All the models (except ECHMERIT) overestimate Hg(0) concentrations at ALT in January
490 and February 2013, but reproduce well the average value in December 2013 (Fig. 6a). It is
491 worth noting that the observed mean value in January/February 2013 ($1.24 \pm 0.13 \text{ ng m}^{-3}$) is
492 lower than the value observed in December 2013 ($1.45 \pm 0.07 \text{ ng m}^{-3}$) and lower than the
493 hemispheric background ($1.30 - 1.60 \text{ ng m}^{-3}$ according to Sprovieri et al. (this issue-a)).
494 Additionally, the observed mean value in January/February 2013 is at the low end of values
495 reported at this period of the year at ALT from 2011 to 2014 (Fig. 3, $1.40 \pm 0.16 \text{ ng m}^{-3}$ in
496 2011, $1.32 \pm 0.09 \text{ ng m}^{-3}$ in 2012, and $1.47 \pm 0.12 \text{ ng m}^{-3}$ in 2014). The inter-annual



497 variability of observed Hg(0) concentrations at ALT is not captured by models. Modeled
498 Hg(0) concentrations in January/February range from 1.48 ± 0.03 in 2014 to 1.54 ± 0.03 ng
499 m^{-3} in 2011 and 2012 with GEOS-C hem and from 1.54 ± 0.06 in 2012 to 1.58 ± 0.04 ng m^{-3}
500 in 2013 with GEM-MACH-Hg. Similarly, the inter-annual variability of modeled Hg(0)
501 concentrations is low at other Arctic sites (Fig. 7a). The wintertime inter-annual variability of
502 observed Hg(0) concentrations might be driven by meteorology and mercury emissions in
503 mid-latitudes. However, the AMAP/UNEP (2010) global inventory of mercury anthropogenic
504 emissions (annual mean emission fields) was used for all simulated years (2011-2014) in both
505 GEOS-Chem and GEM-MACH-Hg, preventing the consideration of inter-annual changes in
506 anthropogenic emissions.

507 **b) Spring**

508 Springtime reflects the lowest Hg(0) concentrations at ALT, SND, and NYA due to the
509 occurrence of AMDEs (see section 3.1.1.2). This minimum is well reproduced by GEM-
510 MACH-Hg, GEOS-Chem, and GLEMOS at all three stations, but not reproduced by
511 ECHMERIT (Fig. 6a). It should be noted that there is no parameterization of AMDEs in the
512 latter. Interestingly, GLEMOS predicts a similar springtime minimum at AND in
513 contradiction with the seasonal pattern observed at this station (see section 3.1.1.2). This
514 discrepancy can likely be attributed to uncertainties in Br fields extracted from p-TOMCAT.

515 As discussed in section 3.1.1.2, AMDEs were less frequent at ALT in 2014. This lower
516 occurrence frequency is fairly well reproduced by GEM-MACH-Hg (61 % (2011), 43 %
517 (2012), 53 % (2013), and 36 % (2014)), but not at all by GEOS-Chem (4 % (2011), 6 %
518 (2012), 13 % (2013), and 37 % (2014)). A temperature-dependence of BrO concentrations is
519 implemented in GEM-MACH-Hg and Br₂ is assumed to occur only over consolidated sea-ice
520 which would change with changing meteorological conditions. Conversely, a constant value
521 of 5 pptv of BrO is added in the springtime Arctic boundary layer into GEOS-Chem v9-02.
522 However, updates to Arctic mercury processes will be implemented in v11-01 based on
523 Fisher et al. (2012) and Fisher et al. (2013) ([http://wiki.seas.harvard.edu/geos-
524 chem/index.php/Mercury#Updates_to_Arctic_Hg_processes](http://wiki.seas.harvard.edu/geos-chem/index.php/Mercury#Updates_to_Arctic_Hg_processes)). BrO concentrations will
525 depend on temperature according to a relationship chosen to optimize spring Hg(0)
526 concentrations and the shift of peak depletion at ALT from May to April (see section 3.1.1.2).
527 It should also be noted that GEOS-Chem relies on GEOS-5 and GEOS-FP meteorological
528 fields in 2011-2013 and 2014, respectively. Simulations in Polar Regions can be very
529 sensitive to subtle changes in meteorological fields, especially during the AMDEs season,



530 which could at least partly explain the inter-annual variability of modeled AMDEs occurrence
531 frequencies.

532 Based on the work by Moore et al. (2014) showing the impact of sea-ice leads on AMDEs
533 (AMDEs might be favored by consolidated sea-ice cover, see section 3.1.1.2), real-time
534 distribution of sea-ice dynamics including presence of leads is needed. Contrarily to
535 conclusions by Moore et al. (2014), a recent modeling study (Chen et al., 2015) carried out
536 using GEOS-Chem v9-02 – but including an ice/snow module and riverine inputs as described
537 by Fisher et al. (2012) and Fisher et al. (2013) – showed that increasing sea ice lead
538 occurrence increases the frequency of AMDEs. These contradictory results highlight the fact
539 that further work is needed regarding the degree to which sea-ice dynamics across the Arctic
540 alters mercury chemistry in spring.

541 **c) Summer**

542 All the models (except ECHMERIT in which polar processes are not implemented) capture,
543 to some extent, the summertime Hg(0) enhancement. GLEMOS clearly underestimates
544 summertime mean concentrations at ALT and SND (Fig. 6a). This can be attributed to
545 missing reemissions and/or oceanic evasion. As mentioned in section 3.1.1.3, Dastoor and
546 Durnford (2014) suggested two distinct summertime maxima: a first one supported by
547 revolatilization from snowpack/meltwaters occurring from the end of May to mid-June at
548 ALT, and in June at NYA; a second one supported by oceanic evasion from mid-July to early
549 August at ALT and NYA. GEOS-Chem gives a summer maximum in June instead of July at
550 ALT, SND, and NYA. This time-lag might result from the fact that oceanic evasion from
551 the Arctic Ocean is not implemented in v9-02. v11-01 of the model will include, among other
552 updates, new present-day (2009) fields for net primary productivity (NPP) based on Jin et al.
553 (2012), a UV-B dependence for Hg(II) reduction in seawater based on results of O'Driscoll et
554 al. (2006), updated Hg(0) emissions from snow, and a source of mercury from the snowpack
555 to the Arctic Ocean at the onset of snowmelt. In order for the models to reproduce the inter-
556 annual variability of Hg(0) concentrations, real-time distribution of areas of ice-free surface
557 waters along with the type of surface (ice/snow/snow-free bedrock) are needed.

558 **3.1.2.2 Reactive Mercury and deposition**

559 Year 2013 modeled monthly-averaged RM concentrations and wet/dry deposition are
560 displayed in Fig. 8a. GEOS-Chem, GEM-MACH-Hg, and GLEMOS predict increased RM
561 concentrations in spring, during the AMDEs season, consistent with the observed pattern at



562 ALT (Fig. 5) and NYA (Wang, 2015). The fact that ECHMERIT does not capture the spring
563 enhancement is not surprising since the model does not implement any chemistry specific to
564 Polar Regions. GLEMOS also predicts a RM spring maximum at AND, in line with the
565 modeled Hg(0) spring minimum at this site (Fig. 6a). As discussed in section 3.1.2.1.b, this
566 can likely be attributed to uncertainties in Br fields extracted from p-TOMCAT. Long-term
567 measurements of RM in the Arctic are scarce and limited to ALT and NYA (data not
568 presented here). According to Fig. 8a, all four models underestimate RM concentrations at
569 ALT from at least January to April 2013. Similarly, the comparison of modeled RM
570 concentrations at NYA with annual averages reported by Steen et al. (2011) and Wang (2015)
571 suggest an underestimation of the concentrations by GEOS-Chem, GEM-MACH-Hg, and
572 ECHMERIT.

573 According to the models, deposition of mercury peaks in spring at ALT and SND, consistent
574 with the RM spring maximum. The deposition of mercury during AMDEs depends on
575 temperature, relative humidity and aerosol contribution (Cobbett et al., 2007), and is higher
576 when the atmospheric conditions favor the formation of RGM over Hg(p) (see section
577 3.1.1.2). Therefore, as suggested by Steffen et al. (2015), prevailing atmospheric conditions
578 must be fully characterized in order to accurately evaluate the deposition of mercury. GEOS-
579 Chem and GLEMOS both predict higher dry deposition in spring at NYA. Wet deposition is
580 largely driven by precipitation – RM being readily scavenged by rain or snow, whereas dry
581 deposition depends on the boundary layer stability and the type of the underlying surface
582 (Cadle, 1991). Deposition of mercury in the Arctic is typically inferred from concentrations of
583 total mercury in the snowpack (e.g., Steffen et al., 2014) or from a Hg(0) flux gradient method
584 (Steffen et al., 2002; Brooks et al., 2006; Cobbett et al., 2007; Steen et al., 2009), and not
585 through direct measurement of wet and dry deposition, making it difficult to evaluate the
586 accuracy of models predictions. To the best of our knowledge, NYA is the only site out of the
587 four Arctic sites where wet deposition measurements have been reported (Sprovieri et al., this
588 issue-b). From May to December 2013, the observed net wet deposition flux is equal to $0.9 \mu\text{g m}^{-2}$
589 while modeled fluxes amount to 1.7, 3.2, 2.8, and $2.4 \mu\text{g m}^{-2}$ according to GLEMOS,
590 GEOS-Chem, GEM-MACH-Hg, and ECHMERIT, respectively. All four models overestimate
591 the wet deposition flux. Interestingly, all four models also overestimate the amount of
592 precipitation (by a factor of 2.0, 2.2, 2.1, and 1.1, respectively. Data not shown). Several
593 studies showed that the form of precipitation (rain vs. snow) influences the collection
594 efficiency of the sampler. Lynch et al. (2003) and Prestbo and Gay (2009) found that the



595 annual collection efficiency is 89 % and 87.1 ± 6.5 %, respectively, at cold weather sites of
596 the United States and Canada experiencing snowfall in winter vs 98.8 ± 4.3 % at warm
597 weather sites (Prestbo and Gay, 2009). Assuming an annual 89 % collection efficiency of
598 snow at NYA does not narrow the gap between observed and modeled amounts of
599 precipitation. However, an annual 89 % collection efficiency at NYA seems generous
600 considering that snow falls year round and that strong wind ($> 10 \text{ m s}^{-1}$) and blowing snow are
601 frequent, especially in winter (Maturilli et al., 2013).

602 3.2 Antarctic sites

603 3.2.1 Observations

604 Fig. 2b shows monthly box plots of all data collected in Antarctica (ground-based sites and
605 cruises). Hg(0) concentrations from the ANT cruises displayed in Fig.2b refer to data
606 collected when R/V Polarstern operated within the marginal sea ice region (8 July – 23 July
607 2013, 25 July – 9 August 2013, 28 August – 5 October 2013) (Nerentorp Mastromonaco et
608 al., 2016). Similarly, Hg(0) concentrations from the OSO cruise refer to data collected at
609 latitude $> 60^\circ\text{S}$. Hg(0) concentrations measured during the ANT and OSO cruises are
610 somewhat higher than values at ground-based Antarctic sites. The average value at Antarctic
611 sites is $0.96 \pm 0.32 \text{ ng m}^{-3}$, i.e. 35% lower than the average value at Arctic sites (see section
612 3.1). This result is consistent with the North-to-South Hg(0) decreasing gradient reported by
613 Sprovieri et al. (this issue-a), and with values reported at Southern Hemisphere mid-latitudes
614 sites (Angot et al., 2014; Slemr et al., 2015).

615 The Hg(0) concentration data from the three Antarctic ground-based sites for the period 2011-
616 2015 are presented as monthly box and whisker plots in Fig. 9. Information regarding
617 annually- and monthly-based statistics at the three sites can be found in Tables 2 and 3,
618 respectively. The annual medians for 2011-2015 at TR and 2012-2015 at DDU (Table 2)
619 suggest a low inter annual variability in the distribution of Hg(0) concentrations. Conversely,
620 Hg(0) concentrations are notably higher in 2015 than in 2012 and 2013 at DC. This trend is
621 more apparent from Fig. 9b, especially from March to September. It is worth noting that in
622 2015 measurements were performed at a different location within the “clean area” (the
623 instrument was moved from one shelter to another). Additionally, following the January 2014
624 instrument failure, a new Tekran instrument operated in 2015. The combination of these two
625 elements likely, at least partly, explains the offset observed in 2015. Despite this offset, the
626 seasonal trends of Hg(0) repeat from year to year at DC (see below).



627 The mean seasonal variation of Hg(0) concentrations at Antarctic ground-based sites is
628 displayed in Fig. 4b. Summer refers to November – February, fall to March – April, winter to
629 May – August, and spring to September – October. At TR, the Hg(0) concentrations are
630 significantly (p value < 0.0001 , Mann-Whitney test) higher in winter ($0.98 \pm 0.06 \text{ ng m}^{-3}$) than
631 in summer ($0.89 \pm 0.29 \text{ ng m}^{-3}$), in good agreement with the seasonal variation reported at TR
632 by Pfaffhuber et al. (2012) from February 2007 to June 2011, and at Neumayer (NM) by
633 Ebinghaus et al. (2002). Contrarily, Hg(0) concentrations at DDU are slightly but significantly
634 (p value < 0.0001 , Mann-Whitney test) higher in summer ($0.88 \pm 0.32 \text{ ng m}^{-3}$) than in winter
635 ($0.84 \pm 0.11 \text{ ng m}^{-3}$). On the high-altitude Antarctic plateau at DC, Hg(0) concentrations
636 exhibit a distinct maximum in fall ($1.45 \pm 0.27 \text{ ng m}^{-3}$) and a minimum in summer ($0.78 \pm$
637 0.46 ng m^{-3}). The mechanisms which cause the seasonal variation of Hg(0) concentrations at
638 Antarctic sites are discussed in the following sections.

639 3.2.1.1 The winter mysteries

640 Hg(0) concentrations at TR remain at a fairly constant level of $0.98 \pm 0.06 \text{ ng m}^{-3}$ in average
641 from April to August (Fig. 2b). This result is in good agreement with observations at
642 Neumayer (Ebinghaus et al., 2002). Pfaffhuber et al. (2012) attributed this phenomenon to the
643 lack of photochemical oxidation processes during the polar night. Conversely, Hg(0)
644 concentrations exhibit a gradual 30% decrease at DC, from 1.48 ± 0.19 in average in April to
645 $0.98 \pm 0.20 \text{ ng m}^{-3}$ in August. This decreasing trend remains unexplained and possibly results
646 from the dry deposition of Hg(0) onto the snowpack (Angot et al., 2016b). In 2013,
647 measurements were performed at various height levels above the snow surface. Interestingly,
648 Angot et al. (2016b) reported a steeper decrease of Hg(0) concentrations close to the snow
649 surface suggesting that the snowpack may act as a sink for mercury. Similarly, a gradual 20%
650 decrease in Hg(0) concentrations is observed at DDU, from 0.94 ± 0.07 in average in April to
651 $0.72 \pm 0.10 \text{ ng m}^{-3}$ in August (Fig. 2b). Based on an analysis of air mass back trajectories,
652 Angot et al. (2016a) suggested that this decreasing trend at DDU most likely results from
653 reactions occurring within the shallow boundary layer on the Antarctic plateau, subsequently
654 transported toward the coastal margins by katabatic winds. DDU is most of the time
655 influenced by inland air masses whereas several studies showed that stations such as NM are
656 not significantly impacted by air masses originating from the Antarctic plateau (Helmig et al.,
657 2007; Legrand et al., 2016b) explaining why concentrations remain rather stable at NM and
658 TR throughout winter.



659 Hg(0) concentration exhibits abrupt increases when moist and warm air masses from lower
660 latitudes occasionally reach the three ground-based Antarctic stations. At DDU, such events
661 are concomitant with an enhanced fraction of oceanic air masses reaching the site according
662 to the HYSPLIT model simulations, and with increased sodium concentrations (Angot et al.,
663 2016a). At DC, these advections of warm and moist air masses are confirmed by an increase
664 of temperature at 10 m a.g.l. and a high integrated water vapor column (Angot et al., 2016b).
665 Finally, based on a statistical analysis of source and sink regions, Pfaffhuber et al. (2012)
666 showed that transport from lower-latitude regions are frequently associated with the highest
667 Hg(0) concentrations at TR.

668 During the winter expedition ANTXXIX/6 on board R/V Polarstern over the Weddell Sea
669 (Fig. 1), Nerentorp Mastromonaco et al. (2016) observed depletions of Hg(0) characterized by
670 strong correlations with O₃. This is the first evidence of Hg(0) depletions occurring in winter.
671 The authors propose a dark mechanism involving Br₂. AMDEs in Antarctica are operationally
672 defined as Hg(0) concentrations below 0.60 ng m⁻³ (Pfaffhuber et al., 2012). Based on this
673 threshold and on the O₃ signal, there is no evidence of Hg(0) depletions occurring during
674 months of complete darkness at the three ground-based Antarctic sites.

675 3.2.1.2 Springtime AMDEs

676 Before going further, it should be noted that TR is not a coastal station. It is located at an
677 elevation of 1275 m and approximately 220 km from the Antarctic coast. Contrarily, DDU is
678 located on a small island about one km offshore from the Antarctic mainland.

679 AMDEs are observed at TR in positive correlation with O₃ (r up to 0.56, p value < 0.001,
680 Spearman test). Based on the 0.60 ng m⁻³ threshold (see previous section), AMDEs occur in 2
681 % of the springtime observations, in line with the occurrence frequency of 5% reported by
682 Pfaffhuber et al. (2012) from February 2007 to June 2011. Based on a statistical analysis of
683 source and sink regions, Pfaffhuber et al. (2012) indicated that the spring Hg(0) sink, caused
684 by AMDEs, is mainly located within sea ice dense areas surrounding Queen Maud Land.
685 AMDEs at TR are weaker and less frequent when compared to the Arctic (see section 3.1.1.2)
686 likely partly due to the location of the station not being exposed directly to depletion events
687 but rather to transport of mercury-depleted air masses (Pfaffhuber et al., 2012). In contrast,
688 AMDEs occur in 28 % of the observations from 28 August to 5 October 2013 during the
689 spring expedition ANTXXIX/7 over sea ice areas of the Weddell Sea. At DDU, on the other
690 side of the Antarctic continent, data covering the spring period are scarce (Table 3). As
691 indicated by Angot et al. (2016a), the absence of depletions in spring 2012 tends to suggest



692 that AMDEs, if any, are not very frequent at DDU. Several studies reported a less efficient
693 bromine chemistry in East compared to West Antarctica due to a less sea-ice coverage (Theys
694 et al., 2011; Legrand et al., 2016a). However, Angot et al. (2016a) reported low Hg(0)
695 concentrations ($0.71 \pm 0.11 \text{ ng m}^{-3}$) and a significant positive correlation with O_3 (r up to 0.65,
696 p value < 0.0001 , Spearman test) in springtime oceanic air masses, likely due to bromine
697 chemistry.

698 3.2.1.3 Boundary layer dynamics on the Antarctic plateau in fall

699 The fall maximum at DC likely partly results from a low boundary layer oxidative capacity
700 under low solar radiation limiting Hg(0) oxidation. Additionally, at DC, weak turbulence and
701 mixing, and strong temperature gradients near the surface are favored by light wind and clear
702 sky conditions (Argentini et al., 2013). The surface-based temperature inversions were
703 characterized by Pietroni et al. (2012) over the course of a year. In summer, a convective
704 boundary layer characterized by a maximum depth of 200-400 m (Argentini et al., 2005)
705 develops around midday. In winter, strong temperature inversions allow for a mixing depth of
706 a few tens of meters only. Based on the limited area model MAR (Modèle Atmosphérique
707 Régional), Angot et al. (2016b) indicated that the fall distinct maximum of Hg(0)
708 concentrations is concomitant with the time when the boundary layer lowers to ~ 50 m in
709 average and no longer exhibits a pronounced diurnal cycle. Hg(0) is thus suddenly dispersed
710 into a reduced volume of air, limiting the dilution. Similarly, several studies showed that NO_x
711 mixing ratios are enhanced when the boundary layer is shallow (Neff et al., 2008; Frey et al.,
712 2013).

713 3.2.1.4 Extremely active processes in summertime

714 Summertime Hg(0) concentrations at the three ground-based sites exhibit a high variability
715 (Fig. 2b), suggesting extremely active processes at this time of the year. Undetected from
716 March to October, a diurnal cycle characterized by a noon Hg(0) maximum is observed in
717 summer at DDU and DC over the 2012-2015 period (Angot et al., 2016a; Angot et al.,
718 2016b). At DC (DDU), Hg(0) concentrations range from $\sim 0.6 \text{ ng m}^{-3}$ ($\sim 0.7 \text{ ng m}^{-3}$) on
719 average at night to $\sim 1.0 \text{ ng m}^{-3}$ ($\sim 1.1 \text{ ng m}^{-3}$) on average around midday. Conversely, there is
720 no diurnal variation in Hg(0) concentrations at TR, in good agreement with observations
721 reported by Pfaffhuber et al. (2012) from February 2007 to June 2011. Similarly, there is no
722 mention of a daily cycle at NM, Terra Nova Bay, and McMurdo where summer campaigns
723 were carried out (Ebinghaus et al., 2002; Temme et al., 2003; Sprovieri et al., 2002; Brooks
724 et al., 2008b). The absence of diurnal cycle at TR can be attributed to the absence of



725 sources/sinks for Hg(0) with a diurnal cycle in the vicinity of the site (Pfaffhuber et al., 2012).
726 The mean summertime Hg(0) concentration is significantly (p value < 0.0001 , Mann-Whitney
727 test) lower at DC ($0.78 \pm 0.46 \text{ ng m}^{-3}$) than at DDU ($0.88 \pm 0.32 \text{ ng m}^{-3}$) and TR (0.89 ± 0.29
728 ng m^{-3}), suggesting a more intense oxidation of Hg(0). The boundary layer oxidative capacity
729 has been shown to be high in summer on the Antarctic plateau with elevated levels of OH, O₃,
730 NO_x, and RO₂ radicals (Davis et al., 2001; Grannas et al., 2007; Eisele et al., 2008; Kukui et
731 al., 2014; Frey et al., 2015). Angot et al. (2016b) performed Hg(0) measurements in both the
732 atmospheric boundary layer and the interstitial air of the snowpack, and analyzed total
733 mercury in surface snow samples. The authors, in good agreement with Brooks et al. (2008a)
734 and Dommergue et al. (2012), suggested that the observed summertime Hg(0) diurnal cycle at
735 DC might be due to a dynamic daily cycle of Hg(0) oxidation, deposition to the snowpack,
736 and reemission from the snowpack. Similarly, a recent study (Wang et al., 2016) reported a
737 Hg(0) diurnal cycle at Kunlun station (80°25'S, 77°6'E) located near Dome A (80°22'S,
738 77°27'E) – the highest elevation point on the Antarctic plateau (4090 m). This suggests that
739 the dynamic daily cycle of Hg(0) oxidation, deposition to the snowpack, and reemission from
740 the snowpack probably occurs throughout the Antarctic plateau. Based on an analysis of air
741 mass back trajectories, Angot et al. (2016a) showed that measurements at DDU on the East
742 Antarctic coast are dramatically influenced by air masses exported from the Antarctic Plateau
743 by strong katabatic winds. The advection of inland air masses enriched in oxidants – NO_x, O₃,
744 and OH (Grilli et al., 2013; Kukui et al., 2012) – and Hg(II) species likely results in the build-
745 up of an atmospheric reservoir of Hg(II) species at DDU, as supported by elevated levels of
746 total mercury in surface snow samples (Angot et al., 2016a). The diurnal cycle observed at
747 DDU – regardless of wind speed and direction – might result from a local dynamic cycle of
748 oxidation/deposition/reemission in the presence of elevated levels of Hg(II) species along
749 with emissions of mercury from ornithogenic soils – formed by an accumulation of penguin
750 excreta.

751 Hg(0) depletion events occur each year in summer at DC with Hg(0) concentrations
752 remaining low ($\sim 0.40 \text{ ng m}^{-3}$) for several weeks. These depletion events do not resemble to
753 the ones observed in the Arctic. They are not associated with depletions of O₃, and occur as
754 air masses stagnate over the Plateau which could favor an accumulation of oxidants within the
755 shallow boundary layer (Angot et al., 2016b). At TR, Pfaffhuber et al. (2012) reported
756 episodic low Hg(0) concentrations in summer, anti-correlated with O₃, and associated with the
757 transport of inland air masses. Results at TR (Pfaffhuber et al., 2012) and DDU (Angot et al.,



758 2016a), along with observations from earlier studies at other coastal Antarctic sites (Sprovieri
759 et al., 2002; Temme et al., 2003), demonstrate that the inland atmospheric reservoir can
760 influence the cycle of atmospheric mercury at a continental scale, especially in areas
761 influenced by recurrent katabatic winds.

762 Additionally, Pfaffhuber et al. (2012) indicated that the ocean is a source of mercury to TR.
763 Similarly, at DDU, Angot et al. (2016a) reported elevated ($1.04 \pm 0.29 \text{ ng m}^{-3}$) Hg(0)
764 concentrations in oceanic air masses along with a significant positive correlation between
765 Hg(0) and the daily-averaged percentage of oceanic air masses ($r = 0.50$, p value < 0.0001 ,
766 Spearman test). These results are in line with the summer Hg(0) enhancement in the Arctic
767 likely partly due to oceanic evasion from ice-free open waters (see section 3.1.1.3).

768 **3.2.2 Comparison with models**

769 Table 4 displays goodness-of-fit statistics between monthly-averaged modeled and observed
770 data in 2013. ECHMERIT slightly underestimates Hg(0) concentrations at the three ground-
771 based Antarctic sites. Contrarily, the three other global models overestimate Hg(0) levels,
772 suggesting an underestimation of sinks. The ability of the four models to reproduce the
773 observed seasonality of Hg(0) concentrations at ground-based Antarctic sites in 2013 is
774 shown in Fig. 6b and discussed in the following sections. The inter-annual variability of the
775 monthly Hg(0) concentration distribution at Antarctic ground-based sites as simulated by
776 GEM-MACH-Hg and GEOS-Chem is displayed in Fig. 7b while Table 5 shows the percent
777 bias between hourly-averaged modeled and observed data on a seasonal basis from 2011 to
778 2014.

779 **3.2.2.1 Seasonal variation**

780 **a) Winter**

781 GEOS-Chem, GEM-MACH-Hg, and GLEMOS overestimate year 2013 Hg(0) concentrations
782 in winter at the three ground-based stations (Fig. 6a). This trend repeats year after year for
783 GEOS-Chem and GEM-MACH-Hg (Table 5). The most striking result, however, is the
784 modeled gradual increase of Hg(0) concentrations over the course of winter at the three
785 ground-based sites according to ECHMERIT, GEOS-Chem, and GEM-MACH-Hg. A mean
786 gradual increase of 9 %, 19 %, and 11 % is predicted by the three models, respectively, from
787 May to August. GLEMOS, however, predicts a mean gradual decrease of 5 % over the course
788 of winter at the three sites. It is to be noted (see section 3.2.1.1) that Hg(0) concentrations are
789 constant from May to August at TR, exhibit a gradual 30 % decrease at DC possibly due to



790 the dry deposition of Hg(0), and a gradual 20 % decrease at DDU due to advection of inland
791 air masses. All in all, the four models misrepresent the decreasing trend at DC and DDU. This
792 might be due to several factors including underestimation of concentrations of oxidants over
793 the East Antarctic plateau at this period of the year, omission of heterogeneous mechanisms,
794 and significant bias in Southern Hemisphere emissions, including oceanic evasion. The strong
795 increase (19 %) of Hg(0) concentrations from May to August predicted by GEOS-Chem is not
796 restricted to the Antarctic continent but is obtained for the whole Southern Hemisphere (Fig. 3
797 in Song et al., 2015). The emission inversion performed by Song et al. (2015) overturns the
798 seasonality of oceanic emissions and better reproduces the ground-based Hg(0) observations
799 in the Southern Hemisphere mid-latitudes and at TR. Further work, including sensitivity tests,
800 is needed to explain the discrepancies between observed and modeled trends.

801 Additionally, all of the four models are unable to capture the differences in trends observed at
802 the three ground-based sites (constant vs. decreasing concentrations). As discussed in section
803 3.2.1.1, TR, contrarily to DDU, is not significantly influenced by inland air masses. This
804 large-scale airflow pattern will have to be captured by models in order to better reproduce
805 observations. Interestingly, Zatko et al. (2016) calculated the annual mean surface wind
806 convergence/divergence over the Antarctic continent using GEOS-Chem. The results –
807 consistent with those by Parish and Bromwich (1987) and Parish and Bromwich (2007) –
808 correctly indicate that the large-scale airflow pattern in Antarctica flows from the East
809 Antarctic plateau towards the coastal margins and accurately highlight major regions of wind
810 convergence. The findings from this study can be used as the basis for future research.

811 **b) Spring**

812 Based on the 0.60 ng m^{-3} threshold, GEM-MACH-Hg and GEOS-Chem do not predict any
813 AMDE at TR over the 2011-2014 period. Considering the low occurrence frequency based on
814 observations (2 %, see section 3.2.1.2), this result is not unreasonable. Similarly, GEM-
815 MACH-Hg does not predict any AMDE at DDU. However, GEOS-Chem predicts AMDEs in
816 1.5 % of the springtime observations at DDU. This over-prediction of AMDEs at DDU likely
817 results from the constant value of 5 pptv of BrO added in the springtime Antarctic boundary
818 layer. While Saiz-Lopez et al. (2007) reported a spring maximum of up to 7 pptv at Halley
819 Station ($75^{\circ}35'S$, $26^{\circ}30'W$, West Antarctic coast), Legrand et al. (2016a) suggested a BrO
820 mixing ratio ≤ 1 pptv at DDU (East Antarctic coast) in spring using an off-line chemistry
821 transport model. Based on the oxygen and nitrogen isotope analysis of airborne nitrate,
822 Savarino et al. (2007) provided further evidence for low BrO levels in the vicinity of DDU.

823 **c) Fall**

824 None of the four models capture the fall maximum at DC (Fig. 6b). While a spatially and
825 temporally resolved distribution of concentrations of oxidants on the East Antarctic Plateau is
826 needed, the boundary layer dynamics must also be taken into account. Based on the work by
827 Lin and McElroy (2010), Zatzko et al. (2016) incorporated a calculation of the boundary layer
828 height across Antarctica and Greenland into GEOS-Chem. One could also rely on model
829 outputs from the limited area model MAR, validated against observations at DC (Gallée and
830 Gorodetskaya, 2010; Gallée et al., 2015). This model agrees very well with observations and
831 provides reliable and useful information about surface turbulent fluxes, vertical profiles of
832 vertical diffusion coefficients and boundary layer height.

833 **d) Summer**

834 The daily variation of Hg(0) concentrations was investigated based on hourly-averaged data
835 provided by GEOS-Chem and GEM-MACH-Hg. The two models are not able to reproduce
836 the noon maximum observed at DC and DDU in summer (3.2.1.4), suggesting that the
837 dynamic daily cycle of deposition and reemission at the air/snow interface is not captured by
838 the models. The bidirectional exchange of Hg(0) is complex and influenced by multiple
839 environmental variables (e.g., UV intensity, temperature, atmospheric turbulence, presence of
840 reactants) limiting the accuracy of flux modeling (Zhu et al., 2016). The work carried out by
841 Durnford et al. (2012) in the Arctic and by Zatzko et al. (2016) in Antarctica could be good
842 starting points for future research. The former developed a new dynamic physically-based
843 snowpack model to determine the fate of mercury deposited onto snowpacks; the latter
844 incorporated an idealized snowpack along with a snow radiative transfer model (Zatzko et al.,
845 2013) into GEOS-Chem to investigate the impact of snow nitrate photolysis on the boundary
846 layer chemistry across Antarctica.

847 **3.2.2.2 Reactive mercury and deposition**

848 According to Fig. 8b, ECHMERIT predicts low RM concentrations during the whole 2013
849 year at the three ground-based stations (annual averages of 10, 7, and 6 pg m⁻³ at TR, DC, and
850 DDU, respectively). GEOS-Chem predicts a peak in spring at the three sites (up to ~ 160 pg
851 m⁻³ in average October at DC), and quite elevated concentrations in summer and fall (~ 85 pg
852 m⁻³ in average). GEM-MACH-Hg predicts increased concentrations in summer at TR and
853 DDU only. Finally, GLEMOS predicts a more intense summer peak at DC (up to ~ 130 pg m⁻³
854 in average in November) than at DDU and TR. Measurements of RM are scarce in



855 Antarctica and have never been reported on a year-round basis. RM concentrations ranging
856 from 100 to 1000 pg m^{-3} have been reported in summer at South Pole (Brooks et al., 2008a)
857 and several studies have reported elevated concentrations at coastal sites in spring during the
858 AMDEs season (165 pg m^{-3} in average at Mc Murdo (Brooks et al., 2008b)) and in summer
859 (mean RGM concentration of 116 pg m^{-3} at Terra Nova Bay (Sprovieri et al., 2002); RGM
860 and Hg(p) concentrations ranging from 5 to $> 300 \text{ pg m}^{-3}$ and from 15 to 120 pg m^{-3} ,
861 respectively, at Neumayer (Temme et al., 2003)). These results along with the seasonal
862 pattern of Hg(0) reported in section 3.2.1 suggest that the atmospheric boundary layer is
863 enriched in RM in summer, especially on the Antarctic plateau, and that the four models tend
864 to underestimate the summertime concentrations. Year-round measurements are needed to
865 further evaluate the accuracy of models predictions.

866 The total (wet + dry) deposition flux for year 2013 is equal to 1.0, 3.3, 2.5, and 3.9 $\mu\text{g m}^{-2} \text{ yr}^{-1}$
867 at TR, 0.8, 1.5, 0.8, and 1.1 $\mu\text{g m}^{-2} \text{ yr}^{-1}$ at DC, and 4.3, 9.7, 9.7, and 4.1 $\mu\text{g m}^{-2} \text{ yr}^{-1}$ at DDU
868 according to GLEMOS, GEOS-Chem, GEM-MACH-Hg, and ECHMERIT, respectively.
869 Deposition during summertime accounts for 73, 53, 68, and 35 % of the total deposition at
870 TR, 58, 50, 37, and 35 % at DC, and 58, 61, 89, and 28 % at DDU according to GLEMOS,
871 GEOS-Chem, GEM-MACH-Hg, and ECHMERIT, respectively. There are no measurements
872 of wet and dry deposition in Antarctica, except Angot et al. (2016b) who reported a Hg(0) dry
873 deposition velocity of $9.3 \cdot 10^{-5} \text{ cm s}^{-1}$ in winter at DC. Similarly to the Arctic (see section
874 3.1.2.2), deposition of mercury is typically inferred from concentrations of total mercury in
875 the snowpack. To the best of our knowledge, results found in Angot et al. (2016b) are the only
876 reported over various seasons. Higher total mercury concentrations in surface snow samples
877 in summer suggest an enhanced deposition at this period of the year. Alternatively, deposition
878 of mercury can be inferred from the biomonitoring of Antarctic macrolichens and mosses.
879 Large-scale and long-term biomonitoring surveys of mercury deposition have been performed
880 in Victoria Land (Bargagli et al., 1993; Bargagli et al., 2005). While all four models predict
881 higher total mercury deposition for year 2013 at high Arctic (ALT, SND, NYA) vs. Antarctic
882 ground-based sites, significantly higher mercury concentrations in Antarctic vs. Northern
883 Hemisphere lichens suggest otherwise (Bargagli et al., 1993).

884 Wet deposition accounts for 14, 53, 47, and 0 % of the total (wet + dry) flux at TR, 35, 7, 14,
885 and 0 % at DC, and 68, 57, 60, and 8 % at DDU according to GLEMOS, GEOS-Chem, GEM-
886 MACH-Hg, and ECHMERIT, respectively. The amount of precipitation is equal to 214, 242,
887 291, and 1127 mm yr^{-1} at TR, 33, 29, 24, and 60 mm yr^{-1} at DC, and 643, 792, 895, and 1751



888 mm yr⁻¹ at DDU according to GLEMOS, GEOS-Chem, GEM-MACH-Hg, and ECHMERIT,
889 respectively. Ground-based measurements of precipitation are sparse and difficult to obtain in
890 Antarctica. Strong winds in coastal regions make it difficult to tell the difference between
891 blowing snow and precipitation (Palermo et al., 2014). On the Antarctic plateau, a significant
892 part of the precipitation falls in the form of ice crystals (diamond dust) under clear-sky
893 conditions (Bromwich, 1988; Fujita and Abe, 2006). Satellite observations of precipitation in
894 Antarctica by active sensors are now possible (Liu, 2008; Stephens et al., 2008). According
895 to Palermo et al. (2014), the mean annual snowfall rate is < 20 mm water equivalent yr⁻¹ at
896 DC, ranges from 20 to 100 mm yr⁻¹ at TR, and from 500 to 700 mm yr⁻¹ at DDU. The low
897 amount of precipitation at DC might, however, be offset by the high mercury-capture
898 efficiency of ice crystals (Douglas et al., 2008) that are frequently observed at that site
899 (Bromwich, 1988; Fujita and Abe, 2006).

900

901 **4 Summary and future perspectives**

902 The data compiled in this study represent the latest available in Polar Regions. While the
903 Arctic is a semi-enclosed ocean almost completely surrounded by land, Antarctica is a land
904 mass – covered with an immense ice shelf – surrounded by ocean. Therefore, the cycle of
905 atmospheric mercury in the two regions presents both similarities and differences. Springtime
906 AMDEs are observed in both regions at coastal sites (see sections 3.1.1.2 and 3.2.1.2). Their
907 frequency and magnitude depend on parameters such as sea-ice dynamics, temperature, and
908 concentration of bromine species, and exhibit a significant but poorly understood inter-annual
909 variability. Additionally, coastal sites in the two regions are influenced by both snowpack
910 reemission and oceanic evasion of Hg(0) in summer (see sections 3.1.1.3 and 3.2.1.4). As
911 evidenced in section 3.1.1.3, the summertime enhancement of Hg(0) concentrations exhibits a
912 significant but little understood inter-annual variability at Arctic sites. The cycle of
913 atmospheric mercury differs between the Arctic and Antarctica, primarily because of their
914 different geography. Arctic sites are significantly influenced by mercury emissions from
915 Northern Hemisphere mid-latitudes – especially in winter (see section 3.1.1.1). Coastal
916 Antarctic sites are significantly influenced by the reactivity of atmospheric mercury observed
917 on the Antarctic Plateau due to the large-scale airflow pattern flowing from the East Antarctic
918 ice sheet towards the coastal margins (katabatic winds). As discussed in section 3.2, the cycle
919 of atmospheric mercury on the Antarctic Plateau is surprising and involves yet unraveled



920 mechanisms in winter and a daily bidirectional exchange of Hg(0) at the air/snow interface in
921 summer.

922 From the comparison of multi-model simulations with observations, we identified whether the
923 processes that affect Hg(0) seasonality and inter-annual variability, including mercury
924 oxidation, deposition and reemission, are appropriately understood and represented in the
925 models. Generally, models reproduce quite fairly the observed seasonality at Arctic sites but
926 fail to reproduce it at Antarctic sites. In order for the models to reproduce the seasonality of
927 Hg(0) concentrations in Antarctica, parameterization of the boundary layer dynamics (see
928 section 3.1.1.3) and of the large-scale airflow pattern (see above) is needed. Moreover,
929 reaction pathways might be missing or inappropriately incorporated in models. Heterogeneous
930 reactions, although poorly understood (Subir et al., 2012), might be required to explain the
931 reactivity on the Antarctic Plateau. Additionally, while NO_x chemistry was shown to prevail
932 upon halogens chemistry in East Antarctica in summer (Legrand et al., 2009; Grilli et al.,
933 2013) it is currently incorporated in none of the four global models.

934 Based on this study, the following research gaps need to be addressed:

935 1. Improving the spatial resolution of RM measurements. There is presently no year-round
936 data available in Antarctica. The Tekran speciation unit suffers from significant biases and
937 interferences, is expensive, labor-intensive, and requires trained operators. Passive samplers,
938 such as Polyethersulfone cation exchange membranes, could provide an alternative (Huang et
939 al., 2014).

940 2. Unraveling of Hg(II) speciation. The exact speciation – expected to vary with space and
941 time – remains unknown. Identification of Hg(II) species in ambient air emerges as one of the
942 priorities for future research (Gustin et al., 2015). Recent advancement on analytical
943 techniques may offer new insights into Hg(II) speciation (Huang et al., 2013; Jones et al.,
944 2016). However, further research is still needed and application of passive samplers for
945 collection and identification of Hg(II) compounds should be tested in various environments
946 and at different times of the year. Such advancement will greatly improve our understanding
947 of atmospheric redox processes.

948 3. Improving the spatial resolution of measurements of total mercury in snow samples. These
949 measurements are an alternative to wet and dry deposition measurements – difficult to
950 perform in Polar Regions.



951 4. Investigation of the fundamental environmental processes driving the inter-annual
952 variability of Hg(0) concentrations, especially at Arctic sites. Further work is needed to
953 establish the degree to which temperature and sea-ice dynamics across the Arctic alters
954 mercury chemistry in spring and summer. This will also open up new opportunities to explore
955 the influence of Climate Change on the cycle of mercury in Polar Regions.

956 5. Investigation (and quantification) of the oceanic fluxes of Hg(0) during oceanographic
957 campaigns across the Arctic and Austral Oceans. This will largely reduce the uncertainty in
958 the mercury budget estimation in Polar Regions.

959 6. Reducing uncertainties in existing kinetic parameters and quantitatively investigate the
960 effect of temperature on the rate constants (Subir et al., 2011). Limited data are available for
961 temperature applicable to atmospheric conditions, especially in Polar Regions. Achieving this
962 will largely reduce uncertainties in atmospheric models.

963 7. Investigation of the influence of atmospheric surfaces (e.g., aerosols, clouds, ice, snow
964 covers, ice crystals). This is a major gap for adequate modeling of mercury cycling (Subir et
965 al., 2012) and studies addressing this are critically needed.

966

967 **Acknowledgements**

968 HA, OM, and AD thank the overwintering crew: S. Aguado, D. Buiron, N. Coillard, G.
969 Dufresnes, J. Guilhermet, B. Jourdain, B. Laulier, S. Oros, A. Thollot, and N. Vogel at DDU,
970 S. Aubin, A. Barbero, N. Hueber, C. Lenormant, and R. Jacob at DC. This work contributed
971 to the EU-FP7 project Global Mercury Observation System (GMOS, www.gmos.eu) and has
972 been supported by a grant from Labex OSUG@2020 (Investissements d'avenir – ANR10
973 LABX56), and the Institut Universitaire de France. Logistical and financial support was
974 provided by the French Polar Institute IPEV (Program 1028, GMOstral). KAP thanks the
975 Norwegian Environmental Agency and the Norwegian Antarctic Research Expeditions for
976 long-term financial support of Norwegian mercury measurements and in particular the
977 technicians J.H. Wasseng and A. Bäcklund at NILU for their excellent care taking of the
978 Tekran monitors. NES and SS acknowledge support from the U.S. National Science
979 Foundation Atmospheric Chemistry Program under grant #1053648.

980



References

- ECMWF: European Centre for Medium-Range Weather Forecasts. <http://www.ecmwf.int/en/forecasts/datasets>, access: 20 January 2016.
- Adams, J. W., Holmes, N. S., and Crowley, J. N.: Uptake and reaction of HOBr on frozen and dry NaCl/NaBr surfaces between 253 and 233 K, *Atmos. Chem. Phys.*, 2, 79-91, 10.5194/acp-2-79-2002, 2002.
- AMAP: Human Health in the Arctic. Arctic Monitoring and Assessment Programme (AMAP), Oslo, Norway, 165pp, 2015.
- Amos, H. M., Jacob, D. J., Holmes, C. D., Fisher, J. A., Wang, Q., Yantosca, R. M., Corbitt, E. S., Galameau, E., Rutter, A. P., Gustin, M. S., Steffen, A., Schauer, J. J., Graydon, J. A., St. Louis, V. L., Talbot, R. W., Edgerton, E. S., Zhang, Y., and Sunderland, E. M.: Gas-particle partitioning of atmospheric Hg(II) and its effect on global mercury deposition, *Atmospheric Chemistry and Physics*, 12, 591-603, 2012.
- Amos, H. M., Sonke, J. E., Obrist, D., Robins, N., Hagan, N., Horowitz, H. M., Mason, R. P., Witt, M. L. I., Hedgecock, I. M., Corbitt, E. S., and Sunderland, E. M.: Observational and modeling constraints on global anthropogenic enrichment of mercury, *Environmental Science and Technology*, 49, 4036-4047, 2015.
- Andersson, M. E. S., J., Gårdfeldt, K., and Linqvist, O.: Enhanced concentrations of dissolved gaseous mercury in the surface waters of the Arctic Ocean, *Marine Chemistry*, 110, 190-194, 2008.
- Angot, H., Barret, M., Magand, O., Ramonet, M., and Dommergue, A.: A 2-year record of atmospheric mercury species at a background Southern Hemisphere station on Amsterdam Island, *Atmospheric Chemistry and Physics* 14, 11461-11473, 2014.
- Angot, H., Dion, I., Vogel, N., Magand, O., Legrand, M., and Dommergue, A.: Atmospheric mercury record at Dumont d'Urville, East Antarctic coast: continental outflow and oceanic influences, *Atmospheric Chemistry and Physics Discussions*, 10.5194/acp-2016-257, in review, 2016a.
- Angot, H., Magand, O., Helmig, D., Ricaud, P., Quennehen, B., Gallée, H., Del Guasta, M., Sprovieri, F., Pirrone, N., Savarino, J., and Dommergue, A.: New insights into the atmospheric mercury cycling in Central Antarctica and implications at a continental scale, *Atmospheric Chemistry and Physics Discussions*, 10.5194/acp-2016-144, in review, 2016b.
- Argentini, S., Viola, A., Sempreviva, A. M., and Petenko, I.: Summer boundary-layer height at the plateau site of Dome C, Antarctica, *Boundary-Layer Meteorology*, 115, 409-422, 2005.
- Argentini, S., Petenko, I., Viola, A., Mastrantonio, G., Pietroni, I., Casasanta, G., Aristidi, E., and Ghenton, C.: The surface layer observed by a high-resolution sodar at Dome C, Antarctica, *Annals of geophysics*, 56, doi:10.4401/ag-6347, 2013.
- Ariya, P. A., Dastoor, A. P., Amyot, M., Schroeder, W. H., Barrie, L., Anlauf, K., Raofie, F., Ryzhkov, A., Davignon, D., Lalonde, J., and Steffen, A.: The arctic: a sink for mercury, *Tellus*, 56B, 397-403, 2004.
- Aspmo, K., Gauchard, P.-A., Steffen, A., Temme, C., Berg, T., Bahlmann, E., Banic, C., Dommergue, A., Ebinghaus, R., Ferrari, C., Pirrone, N., Sprovieri, F., and Wibetoe, G.: Measurements of atmospheric mercury species during an international study of mercury depletion events at Ny-Ålesund, Svalbard, spring 2003. How reproducible are our present methods?, *Atmospheric Environment*, 39, 7607-7619, 2005.



Aspmo, K., Temme, C., Berg, T., Ferrari, C., Gauchard, P.-A., Fäin, X., and Wibetoe, G.: Mercury in the atmosphere, snow and melt water ponds in the north atlantic ocean during Arctic summer, *Environmental Science and Technology*, 40, 4083-4089, 2006.

Balabanov, N. B., Shepler, B. C., and Peterson, K. A.: Accurate Global Potential Energy Surface and Reaction Dynamics for the Ground State of HgBr₂, *The Journal of Physical Chemistry A*, 109, 8765-8773, 10.1021/jp053415l, 2005.

Bargagli, R., Battisti, E., Focardi, S., and Formichi, P.: Preliminary data on environmental distribution of mercury in northern Victoria Land, Antarctica, *Antarctic Science*, 5, 3-8, 1993.

Bargagli, R., Agnorelli, C., Borghini, F., and Monaci, F.: Enhanced deposition and bioaccumulation of mercury in antarctic terrestrial ecosystems facing a coastal polynya, *Environmental Science and Technology*, 39, 8150-8155, 2005.

Barrie, L. A., Hoff, R. M., and Daggupaty, S. M.: Arctic Air Chemistry Proceedings of the Second Symposium The influence of mid-latitude pollution sources on haze in the Canadian arctic, *Atmospheric Environment* (1967), 15, 1407-1419, [http://dx.doi.org/10.1016/0004-6981\(81\)90347-4](http://dx.doi.org/10.1016/0004-6981(81)90347-4), 1981.

Berg, T., Bartnicki, J., Munthe, J., Lattila, H., Hrehoruk, J., and Mazur, A.: Atmospheric mercury species in the European Arctic: measurements and modelling, *Atmospheric Environment*, 35, 2569-2582, 2001.

Berg, T., Sekkesæter, S., Steinnes, E., Valdal, A.-K., and Wibetoe, G.: Springtime depletion of mercury in the European Arctic as observed at Svalbard, *Science of The Total Environment*, 304, 43-51, [http://dx.doi.org/10.1016/S0048-9697\(02\)00555-7](http://dx.doi.org/10.1016/S0048-9697(02)00555-7), 2003a.

Berg, T., Sommar, J., Wängberg, Gardfeldt, K., Munthe, J., and Schroeder, B.: Arctic mercury depletion events at two elevations as observed at the Zeppelin Station and Dirigibile Italia, Ny-Ålesund, spring 2002, *J. Phys. IV France*, 107, 151-154, 2003b.

Berg, T., Aspmo, K., and Steinnes, E.: Transport of Hg from atmospheric mercury depletion events to the mainland of Norway and its possible influence on Hg deposition, *Geophysical research letters*, 35, doi:10.1029/2008GL033586, 2008.

Berg, T., Pfaffhuber, K. A., Cole, A. S., Engelsen, O., and Steffen, A.: Ten-year trends in atmospheric mercury concentrations, meteorological effects and climate variables at Zeppelin, Ny-Alesund, *Atmospheric Chemistry and Physics*, 13, 6575-6586, 2013.

Bey, I., Jacob, D. J., Yantosca, R. M., Logan, J. A., Field, B. D., Fiore, A. M., li, Q., Liu, H. Y., Mickley, L. J., and Schultz, M. G.: Global modeling of tropospheric chemistry with assimilated meteorology: model description and evaluation, *Journal of geophysical research*, 106, 23,073-023,095, 2001.

Bilello, M. A.: Prevailing wind directions in the Arctic Ocean, Corps of Engineers, U. S. Army: Hanover, New Hampshire, 38, 1973.

Bloom, N. S., and Fitzgerald, W. F.: Determination of volatile mercury species at the picogram level by low temperature gas chromatography with cold-vapor atomic fluorescence detection, *Analytica Chimica Acta*, 208, 151-161, 1988.

Bourgeois, Q., and Bey, I.: Pollution transport efficiency toward the Arctic: sensitivity to aerosol scavenging and source regions, *Journal of geophysical research*, 116, 10.1029/2010JD015096, 2011.

Bromwich, D. H.: Snowfall in high southern latitudes, *Rev. Geophys.*, 26, 149-168, <http://dx.doi.org/10.1029/RG026i001p00149>, 1988.



Brooks, S., Saiz-Lopez, A., Skov, H., Lindberg, S. E., Plane, J. M. C., and Goodsite, M. E.: The mass balance of mercury in the springtime arctic environment, *Geophysical research letters*, doi: 10.1029/2005GL025525, 2006.

Brooks, S. B., Arimoto, R., Lindberg, S. E., and Southworth, G.: Antarctic polar plateau snow surface conversion of deposited oxidized mercury to gaseous elemental mercury with fractional long-term burial, *Atmospheric Environment*, 42, 2877-2884, 2008a.

Brooks, S. B., Lindberg, S. E., Southworth, G., and Arimoto, R.: Springtime atmospheric mercury speciation in the McMurdo, Antarctica coastal region, *Atmospheric Environment*, 42, 2885-2893, 2008b.

Cadle, S. H.: Dry Deposition to Snowpacks, in: *Seasonal Snowpacks: Processes of Compositional Change*, edited by: Davies, T. D., Tranter, M., and Jones, H. G., Springer Berlin Heidelberg, Berlin, Heidelberg, 21-66, 1991.

Chen, L., Zhang, Y., Jacob, D. J., Soerensen, A. L., Fisher, J. A., Horowitz, H. M., Corbitt, E. S., and Wang, X.: A decline in Arctic Ocean mercury suggested by differences in decadal trends of atmospheric mercury between the Arctic and northern midlatitudes, *Geophysical research letters*, 42, 10.1002/2015GL064051, 2015.

Cobbett, F. D., Steffen, A., Lawson, G., and Van Heyst, B. J.: GEM fluxes and atmospheric mercury concentrations (GEM, RGM and Hg(p)) in the Canadian Arctic at Alert, Nunavut, Canada (February–June 2005), *Atmospheric Environment*, 41, 6527-6543, <http://dx.doi.org/10.1016/j.atmosenv.2007.04.033>, 2007.

Cole, A. S., and Steffen, A.: Trends in long-term gaseous mercury observations in the Arctic and effects of temperature and other atmospheric conditions, *Atmos. Chem. Phys.*, 10, 4661-4672, 10.5194/acp-10-4661-2010, 2010.

Cole, A. S., Steffen, A., Pfaffhuber, K. A., Berg, T., Pilote, M., Poissant, L., Tordon, R., and Hung, H.: Ten-year trends of atmospheric mercury in the high Arctic compared to Canadian sub-Arctic and mid-latitudes sites, *Atmospheric Chemistry and Physics*, 13, 1535-1545, 2013.

D'Amore, F., Bencardino, M., Cinnirella, S., Sprovieri, F., and Pirrone, N.: Data quality through a web-based QA/QC system: implementation for atmospheric mercury data from the Global Mercury Observation System, *Environmental Science: Processes & Impacts*, 17, 1482-1491, 2015.

Dastoor, A., Ryzhkov, A., Durnford, D., Lehnerr, I., Steffen, A., and Morrison, H.: Atmospheric mercury in the Canadian Arctic. Part II: Insight from modeling, *Science of The Total Environment*, 509–510, 16-27, <http://dx.doi.org/10.1016/j.scitotenv.2014.10.112>, 2015.

Dastoor, A. P., and Larocque, Y.: Global circulation of atmospheric mercury: a modelling study, *Atmospheric Environment*, 38, 147-161, 2004.

Dastoor, A. P., Davignon, D., Theys, N., Van Roozendaal, M., Steffen, A., and Ariya, P. A.: Modeling dynamic exchange of gaseous elemental mercury at polar sunrise, *Environmental Science and Technology*, 42, 5183-5188, 2008.

Dastoor, A. P., and Durnford, D. A.: Arctic ocean: is it a sink or a source of atmospheric mercury?, *Environmental Science and Technology*, 48, 1707-1717, 2014.

Davis, D., Nowak, J. B., Chen, G., Buhr, M., Arimoto, R., Hogan, A., Eisele, F., Mauldin, L., Tanner, D., Shetter, R., Lefer, B., and McMurry, P.: Unexpected high levels of NO observed at South Pole, *Geophysical research letters*, 28, 3625-3628, 2001.



De Simone, F., Gencarelli, C. N., Hedgecock, I. M., and Pirrone, N.: Global atmospheric cycle of mercury: a model study on the impact of oxidation mechanisms, *Environmental Science and Pollution Research*, 21, 4110-4123, 2014.

De Simone, F., Gencarelli, C. N., Hedgecock, I. M., and Pirrone, N.: A Modeling Comparison of Mercury Deposition from current Anthropogenic Mercury Emission Inventories, *Environmental Science & Technology*, 10.1021/acs.est.6b00691, 2016.

Dibble, T. S., Zelig, M. J., and Mao, H.: Thermodynamics of reactions of ClHg and BrHg radicals with atmospherically abundant free radicals, *Atmospheric Chemistry and Physics*, 12, 10271-10279, 2012.

Dommergue, A., Larose, C., Fain, X., Clarisse, O., Foucher, D., Hintelmann, H., Schneider, D., and Ferrari, C. P.: Deposition of Mercury Species in the Ny-Ålesund Area (79°N) and Their Transfer during Snowmelt, *Environmental Science & Technology*, 44, 901-907, 10.1021/es902579m, 2010a.

Dommergue, A., Sprovieri, F., Pirrone, N., Ebinghaus, R., Brooks, S., Courteaud, J., and Ferrari, C. P.: Overview of mercury measurements in the antarctic troposphere, *Atmospheric Chemistry and Physics*, 10, 3309-3319, 2010b.

Dommergue, A., Barret, M., Courteaud, J., Cristofanelli, P., Ferrari, C. P., and Gallée, H.: Dynamic recycling of gaseous elemental mercury in the boundary layer of the antarctic plateau, *Atmospheric Chemistry and Physics*, 12, 11027-11036, 2012.

Donohoue, D. L., Bauer, D., Cossairt, B., and Hynes, A. J.: Temperature and pressure dependent rate coefficients for the reaction of Hg with Br and the reaction of Br with Br: a pulsed laser photolysis-pulsed laser induced fluorescence study, *Journal of physical chemistry*, 110, 6623-6632, 2006.

Douglas, T. A., Sturm, M., Simpson, W. R., Blum, J. D., Alvarez-Aviles, L., Keeler, G. J., Perovich, D. K., Biswas, A., and Johnson, K.: Influence of snow and ice crystal formation and accumulation on mercury deposition to the Arctic, *Environmental Science and Technology*, 42, 1542-1551, 2008.

Douglas, T. A., Loseto, L. L., Macdonald, R. W., Outridge, P. M., Dommergue, A., Poulain, A. J., Amyot, M., Barkay, T., Berg, T., Chételat, J., Constant, P., Evans, M. J., Ferrari, C., Gantner, N., Johnson, M. S., Kirk, J., Kroer, N., Larose, C., Lean, D., Gissel Nielsen, T., Poissant, L., Rognerud, S., Skov, H., Sørensen, S., Wang, F., Wilson, S., and Zdanowicz, C.: The fate of mercury in Arctic terrestrial and aquatic ecosystems, a review, *Environ. Chem.*, 9, 321-355, <http://dx.doi.org/10.1071/EN11140>, 2012.

Driscoll, C. T., Mason, R. P., Chan, H. M., Jacob, D. J., and Pirrone, N.: Mercury as a global pollutant: sources, pathways, and effects, *Environmental Science and Technology*, 47, 4967-4983, 2013.

Dumarey, R., Temmerman, E., Dams, R., and Hoste, J.: The accuracy of the vapour injection calibration method for the determination of mercury by amalgamation/cold vapour atomic spectrometry, *Analytica Chimica Acta*, 170, 337-340, 1985.

Durnford, D., Dastoor, A., Figueras-Nieto, D., and Ryjkov, A.: Long range transport of mercury to the Arctic and across Canada, *Atmospheric Chemistry and Physics*, 10, 6063-6086, 2010.

Durnford, D., Dastoor, A., Ryzhkov, A., Poissant, L., Pilote, M., and Figueras-Nieto, D.: How relevant is the deposition of mercury onto snowpacks? – Part 2: A modeling study, *Atmos. Chem. Phys.*, 12, 9251-9274, 10.5194/acp-12-9251-2012, 2012.



Ebinghaus, R., Kock, H. H., Temme, C., Einax, J. W., Löwe, A. G., Richter, A., Burrows, J. P., and Schroeder, W. H.: Antarctic springtime depletion of atmospheric mercury, *Environmental Science and Technology*, 36, 1238-1244, 2002.

Eisele, F., Davis, D. D., Helmig, D., Oltmans, S. J., Neff, W., Huey, G., Tanner, D., Chen, G., Crawford, J. H., Arimoto, R., Buhr, M., Mauldin, L., Hutterli, M., Dibb, J., Blake, D., Brooks, S. B., Johnson, B., Roberts, J. M., Wang, Y., Tan, D., and Flocke, F.: Antarctic tropospheric chemistry (ANTCI) 2003 overview, *Atmospheric Environment*, 2008, 2749-2761, 2008.

Emmons, L. K., Walters, S., Hess, P. G., Lamarque, J. F., Pfister, G. G., Fillmore, D., Granier, C., Guenther, A., Kinnison, D., Laepple, T., Orlando, J., Tie, X., Tyndall, G., Wiedinmyer, C., Baughcum, S. L., and Kloster, S.: Description and evaluation of the Model for Ozone and Related chemical Tracers, version 4 (MOZART-4), *Geosci. Model Dev.*, 3, 43-67, 10.5194/gmd-3-43-2010, 2010.

Ferrari, C. P., Gauchard, P.-A., Aspmo, K., Dommergue, A., Magand, O., Bahlmann, E., Nagorski, S., Temme, C., Ebinghaus, R., Steffen, A., Banic, C., Berg, T., Planchon, F., Barbante, C., Cescon, P., and Boutron, C. F.: Snow-to-air exchanges of mercury in an arctic seasonal snowpack in Ny-Alesund, Svalbard, *Atmospheric Environment*, 39, 7633-7645, 2005.

Fisher, J. A., Jacob, D. J., Soerensen, A. L., Amos, H. M., Steffen, A., and Sunderland, E. M.: Riverine source of Arctic Ocean mercury inferred from atmospheric observations, *Nature Geosci.*, 5, 499-504, <http://www.nature.com/ngeo/journal/v5/n7/abs/ngeo1478.html#supplementary-information>, 2012.

Fisher, J. A., Jacob, D. J., Soerensen, A. L., Amos, H. M., Corbitt, E. S., Streets, D. G., Wang, Q., Yantosca, R. M., and Sunderland, E. M.: Factors driving mercury variability in the Arctic atmosphere and ocean over the past 30 years, *Global biogeochemical cycles*, 27, 1226-1235, 2013.

Fitzgerald, W. F., and Gill, G. A.: Subnanogram determination of mercury by two-stage gold amalgamation and gas detection applied to atmospheric analysis, *Analytical chemistry*, 51, 1714-1720, 1979.

Frey, M. M., Brough, N., France, J. L., Anderson, P. S., Traulle, O., King, M. D., Jones, A. E., Wolff, E. W., and Savarino, J.: The diurnal variability of atmospheric nitrogen oxides (NO and NO₂) above the Antarctic Plateau driven by atmospheric stability and snow emissions, *Atmospheric Chemistry and Physics*, 13, 3045-3062, 2013.

Frey, M. M., Roscoe, H. K., Kukui, A., Savarino, J., France, J. L., King, M. D., Legrand, M., and Preunkert, S.: Atmospheric nitrogen oxides (NO and NO₂) at Dome C, East Antarctica, during the OPALE campaign, *Atmospheric Chemistry and Physics*, 15, 7859-7875, 2015.

Fujita, K., and Abe, O.: Stable isotopes in daily precipitation at Dome Fuji, East Antarctica, *Geophysical research letters*, 33, <http://dx.doi.org/10.1029/2006GL026936>, 2006.

Gallée, H., and Gorodetskaya, I. V.: Validation of a limited area model over Dome C, Antarctic Plateau, during winter, *Climate Dynamics*, 34, 61-72, 2010.

Gallée, H., Preunkert, S., Argentini, S., Frey, M. M., Genthon, C., Jourdain, B., Pietroni, I., Casasanta, G., Barral, H., Vignon, E., Amory, C., and Legrand, M.: Characterization of the boundary layer at Dome C (East Antarctica) during the OPALE summer campaign, *Atmospheric Chemistry and Physics*, 15, 6225-6236, 2015.



Gårdfeldt, K., Sommar, J., Strömberg, D., and Feng, X.: Oxidation of atomic mercury by hydroxyl radicals and photoinduced decomposition of methylmercury in the aqueous phase, *Atmospheric Environment*, 35, 3039-3047, 2001.

Gauchard, P.-A., Aspö, K., Temme, C., Steffen, A., Ferrari, C., Berg, T., Ström, J., Kaleschke, L., Dommergue, A., Bahlmann, E., Magand, O., Planchon, F., Ebinghaus, R., Banic, C., Nagorski, S., Baussand, P., and Boutron, C.: Study of the origin of atmospheric mercury depletion events recorded in Ny-Ålesund, Svalbard, spring 2003, *Atmospheric Environment*, 39, 7620-7632, <http://dx.doi.org/10.1016/j.atmosenv.2005.08.010>, 2005.

Goodsite, M., Plane, J. M. C., and Skov, H.: Correction to a theoretical study of the oxidation of Hg⁰ to HgBr₂ in the troposphere, *Environmental Science & Technology*, 46, 5262–5262, 2012.

Goodsite, M. E., Plane, J. M. C., and Skov, H.: A theoretical study of the oxidation of Hg⁰ to HgBr₂ in the troposphere, *Environmental Science and Technology*, 38, 1772-1776, 2004.

Grannas, A. M., Jones, A. E., Dibb, J., Ammann, M., Anastasio, C., Beine, H. J., Bergin, M., Bottenheim, J., Boxe, C. S., Carver, G., Chen, G., Crawford, J. H., Domine, F., Frey, M. M., Guzman, M. I., Heard, D. E., Helmig, D., Hoffmann, M. R., Honrath, R. E., Huey, L. G., Hutterli, M., Jacobi, H.-W., Klan, P., Lefer, B., McConnell, J. R., Plane, J. M. C., Sander, R., Savarino, J., Shepson, P. B., Simpson, W. R., Sodeau, J., Von Glasow, R., Weller, R., Wolff, E. W., and Zhu, T.: An overview of snow photochemistry: evidence, mechanisms and impacts, *Atmospheric Chemistry and Physics*, 7, 4329-4373, 2007.

Grilli, R., Legrand, M., Kukui, A., Méjean, G., Preunkert, S., and Romanini, D.: First investigations of IO, BrO, and NO₂ summer atmospheric levels at a coastal East Antarctic site using mode-locked cavity enhanced absorption spectroscopy, *Geophysical research letters*, 40, 791-796, 2013.

Gustin, M. S., Huang, J., Miller, M. B., Peterson, C., Jaffe, D. A., Ambrose, J., Finley, B. D., Lyman, S. N., Call, K., Talbot, R., Feddersen, D., Mao, H., and Lindberg, S. E.: Do we understand what the mercury speciation instruments are actually measuring? Results of RAMIX, *Environmental Science and Technology*, 47, 7295-7306, 2013.

Gustin, M. S., Amos, H. M., Huang, J., Miller, M. B., and Heidecorn, K.: Measuring and modeling mercury in the atmosphere: a critical review, *Atmospheric Chemistry and Physics*, 15, 5697-5713, 2015.

Gustin, M. S., Evers, D. C., Bank, M. S., Hammerschmidt, C. R., Pierce, A., Basu, N., Blum, J., Bustamante, P., Chen, C., Driscoll, C. T., Horvat, M., Jaffe, D., Pacyna, J., Pirrone, N., and Selin, N.: Importance of Integration and Implementation of Emerging and Future Mercury Research into the Minamata Convention, *Environmental Science & Technology*, 50, 2767-2770, [10.1021/acs.est.6b00573](https://doi.org/10.1021/acs.est.6b00573), 2016.

Hall, B.: The gas phase oxidation of elemental mercury by ozone, *Water, Air & Soil Pollution*, 80, 301-315, 1995.

Heidam, N. Z., Wählin, P., and Christensen, J. H.: Tropospheric Gases and Aerosols in Northeast Greenland, *Journal of the Atmospheric Sciences*, 56, 261-278, doi:10.1175/1520-0469(1999)056<0261:TGAAIN>2.0.CO;2, 1999.

Heidam, N. Z., Christensen, J., Wählin, P., and Skov, H.: Arctic atmospheric contaminants in NE Greenland: levels, variations, origins, transport, transformations and trends 1990–2001, *Science of the Total Environment*, 331, 5-28, <http://dx.doi.org/10.1016/j.scitotenv.2004.03.033>, 2004.



Heintzenberg, J., Hansson, H. C., and Lannefors, H.: The chemical composition of arctic haze at Ny-Ålesund, Spitsbergen, *Tellus*, 33, 162-171, 10.1111/j.2153-3490.1981.tb01741.x, 1981.

Helmig, D., Oltmans, S. J., Carlson, D., Lamarque, J.-F., Jones, A., Labuschagne, C., Anlauf, K., and Hayden, K.: A review of surface ozone in the polar regions, *Atmospheric Environment*, 41, 5138-5161, 2007.

Hirdman, D., Aspö, K., Burkhart, J. F., Eckhardt, S., Sodemann, H., and Stohl, A.: Transport of mercury in the Arctic atmosphere: Evidence for a spring-time net sink and summer-time source, *Geophysical research letters*, 36, doi:10.1029/2009GL038345, 2009.

Holmes, C. D., Jacob, D. J., Corbitt, E. S., Mao, J., Yang, X., Talbot, R., and Slemr, F.: Global atmospheric model for mercury including oxidation by bromine atoms, *Atmospheric Chemistry and Physics*, 10, 12037-12057, 2010.

Huang, J., Miller, M. B., Weiss-Penzias, P., and Gustin, M. S.: Comparison of gaseous oxidized mercury measured by KCl-coated denuders, and nylon and cation exchange membranes, *Environmental Science and Technology*, 47, 7307-7316, 2013.

Huang, J., Lyman, S. N., Hartman, J. S., and Gustin, M. S.: A review of passive sampling systems for ambient air mercury measurements, *Environmental Science: Processes & Impacts*, 16, 374-392, 10.1039/C3EM00501A, 2014.

Jaffe, D. A., Lyman, S., Amos, H. M., Gustin, M. S., Huang, J., Selin, N. E., Levin, L., Schure, A., Mason, R. P., Talbot, R., Rutter, A. P., Finley, B., Jaeglé, L., Shah, V., McClure, C., Ambrose, J., Gratz, L., Lindberg, S. E., Weiss-Penzias, P., Sheu, G.-R., Feddersen, D., Horvat, M., Dastoor, A., Hynes, A. J., Mao, H., Sonke, J. E., Slemr, F., Fisher, J. A., Ebinghaus, R., Zhang, B., and Edwards, D. P.: Progress on understanding atmospheric mercury hampered by uncertain measurements, *Environmental Science and Technology*, 48, 7204-7206, doi: 10.1021/es5026432, 2014.

Jin, M., Deal, C., Lee, S. H., Elliott, S., Hunke, E., Maltrud, M., and Jeffery, N.: Investigation of Arctic sea ice and ocean primary production for the period 1992–2007 using a 3-D global ice–ocean ecosystem model, *Deep Sea Research Part II: Topical Studies in Oceanography*, 81–84, 28-35, <http://dx.doi.org/10.1016/j.dsr2.2011.06.003>, 2012.

Jones, C. P., Lyman, S. N., Jaffe, D. A., Allen, T., and O'Neil, T. L.: Detection and quantification of gas-phase oxidized mercury compounds by GC/MS, *Atmos. Meas. Tech.*, 9, 2195-2205, 10.5194/amt-9-2195-2016, 2016.

Jung, G., Hedgecock, I. M., and Pirrone, N.: ECHMERIT V1.0 – a new global fully coupled mercury-chemistry and transport model, *Geosci. Model Dev.*, 2, 175-195, 10.5194/gmd-2-175-2009, 2009.

Kirk, J. L., St. Louis, V. L., and Sharp, M. J.: Rapid Reduction and Reemission of Mercury Deposited into Snowpacks during Atmospheric Mercury Depletion Events at Churchill, Manitoba, Canada, *Environmental Science & Technology*, 40, 7590-7596, doi: 10.1021/es061299+, 2006.

Koop, T., Kapilashrami, A., Molina, L. T., and Molina, M. J.: Phase transitions of sea-salt/water mixtures at low temperatures: implications for ozone chemistry in the polar marine boundary layer, *Journal of geophysical research*, 105, 26393–26402 10.1029/2000JD900413, 2000.

Kos, G., Ryzhkov, A., Dastoor, A., Narayan, J., Steffen, A., Ariya, P. A., and Zhang, L.: Evaluation of discrepancy between measured and modelled oxidized mercury species, *Atmospheric Chemistry and Physics*, 13, 4839-4863, 2013.



Kukui, A., Legrand, M., Ancellet, G., Gros, V., Bekki, S., Sarda-Estève, R., Loisil, R., and Preunkert, S.: Measurements of OH and RO₂ radicals at the coastal Antarctic site of Dumont d'Urville (East Antarctica) in summer 2010-2011, *Journal of geophysical research*, 117, doi:10.1029/2012JD017614, 2012.

Kukui, A., Legrand, M., Preunkert, S., Frey, M. M., Loisil, R., Gil Roca, J., Jourdain, B., King, M. D., France, J. L., and Ancellet, G.: Measurements of OH and RO₂ radicals at Dome C, East Antarctica, *Atmospheric Chemistry and Physics*, 14, 12373-12392, 2014.

Kwon, S. Y., and Selin, N. E.: Uncertainties in Atmospheric Mercury Modeling for Policy Evaluation, *Current Pollution Reports*, 1-12, 10.1007/s40726-016-0030-8, 2016.

Lamborg, C. H., Hammerschmidt, C. R., Bowman, K. L., Swarr, G. J., Munson, K. M., Ohnemus, D. C., Lam, P. J., Heimbürger, L.-E., Rikjensberg, M. J. A., and Saito, M. A.: A global ocean inventory of anthropogenic mercury based on water column measurements, *Nature*, 512, doi:10.1038/nature13563, 2014.

Larose, C., Dommergue, A., De Angelis, M., Cossa, D., Averty, B., Maruszczak, N., Soumis, N., Schneider, D., and Ferrari, C.: Springtime changes in snow chemistry lead to new insights into mercury methylation in the Arctic, *Geochimica et Cosmochimica Acta*, 74, 6263-6275, 2010.

Legrand, M., Preunkert, S., Jourdain, B., Gallée, H., Goutail, F., Weller, R., and Savarino, J.: Year-round record of surface ozone at coastal (Dumont d'Urville) and inland (Concordia) sites in east antarctica, *Journal of geophysical research*, 114, doi:10.1029/2008JD011667, 2009.

Legrand, M., Yang, X., Preunkert, S., and Theys, N.: Year-round records of sea salt, gaseous, and particulate inorganic bromine in the atmospheric boundary layer at coastal (Dumont d'Urville) and central (Concordia) East Antarctic sites, *Journal of geophysical research: atmospheres*, 121, DOI: 10.1002/2015JD024066, 2016a.

Legrand, M. P., S., Savarino, J., Frey, M. M., Kukui, A., Helmig, D., Jourdain, B., Jones, A., Weller, R., Brough, N., and Gallée, H.: Inter-annual variability of surface ozone at coastal (Dumont d'Urville, 2004-2014) and inland (Concordia, 2007-2014) sites in East Antarctica, *Atmospheric Chemistry and Physics Discussions*, doi:10.5194/acp-2016-95, in review, 2016b.

Lin, C.-J., and Pehkonen, S. O.: The chemistry of atmospheric mercury: a review, *Atmospheric Environment*, 33, 2067-2079, 1999.

Lin, J.-T., and McElroy, M. B.: Impacts of boundary layer mixing on pollutant vertical profiles in the lower troposphere: Implications to satellite remote sensing, *Atmospheric Environment*, 44, 1726-1739, <http://dx.doi.org/10.1016/j.atmosenv.2010.02.009>, 2010.

Lindberg, S. E., and Stratton, W. J.: Atmospheric mercury speciation: concentrations and behavior of reactive gaseous mercury in ambient air, *Environmental Science and Technology*, 32, 49-57, 1998.

Lindberg, S. E., Brooks, S., Lin, C.-J., Scott, K., Meyers, T., Chambers, L., Landis, M., and Stevens, R.: Formation of Reactive Gaseous Mercury in the Arctic: Evidence of Oxidation of Hg⁰ to Gas-Phase Hg-II Compounds after Arctic Sunrise, *Water, Air and Soil Pollution: Focus*, 1, 295-302, doi: 10.1023/a:1013171509022, 2001.

Lindberg, S. E., Brooks, S., Lin, C.-J., Scott, K. J., Landis, M. S., Stevens, R. K., Goodsite, M. E., and Richter, A.: Dynamic oxidation of gaseous mercury in the arctic troposphere at polar sunrise, *Environmental Science and Technology*, 36, 1245-1256, 2002.

Lindqvist, O., and Rodhe, H.: Atmospheric mercury - a review, *Tellus*, 37B, 136-159, 1985.



- Liu, G.: Deriving snow cloud characteristics from CloudSat observations, *Journal of geophysical research*, 113, <http://dx.doi.org/10.1029/2007JD009766>, 2008.
- Lu, J. Y., Schroeder, W. H., Barrie, L. A., Steffen, A., Welch, H. E., Martin, K., Lockhart, L., Hunt, R. V., Boila, G., and Richter, A.: Magnification of atmospheric mercury deposition to polar regions in springtime: the link to tropospheric ozone depletion chemistry, *Geophysical research letters*, 28, 3219-3222, 2001.
- Lyman, S. N., Jaffe, D. A., and Gustin, M. S.: Release of mercury halides from KCl denuders in the presence of ozone, *Atmospheric Chemistry and Physics*, 10, 8197-8204, 2010.
- Lynch, J. A., Horner, K. S., and Grimm, J. W.: Atmospheric deposition: spatial and temporal variations in Pennsylvania 2002, Penn State Institutes of the Environment, The Pennsylvania State University, University Park, PA, 231, 2003.
- Maturilli, M., Herber, A., and König-Langlo, G.: Climatology and time series of surface meteorology in Ny-Alesund, Svalbard, *Earth System Science Data*, 5, 155-163, 10.5194/essd-5-155-2013, 2013.
- Moore, C. W., Obrist, D., Steffen, A., Staebler, R. M., Douglas, T. A., Richter, A., and Nghiem, S. V.: Convective forcing of mercury and ozone in the Arctic boundary layer induced by leads in sea ice, *Nature*, 506, 81-84, 10.1038/nature12924, 2014.
- Munthe, J.: The aqueous oxidation of elemental mercury by ozone, *Atmospheric Environment*, 26, 1461-1468, 1992.
- Nash, J. E., and Sutcliffe, J. V.: River flow forecasting through conceptual models part I — A discussion of principles, *Journal of Hydrology*, 10, 282-290, [http://dx.doi.org/10.1016/0022-1694\(70\)90255-6](http://dx.doi.org/10.1016/0022-1694(70)90255-6), 1970.
- Neff, W., Helmig, D., Grachev, A. A., and Davis, D.: A study of boundary layer behavior associated with high NO concentrations at the South Pole using a minisodar, tethered balloon, and sonic anemometer, *Atmospheric Environment*, 42, 2762-2779, 2008.
- Nerentorp Mastromonaco, M., Gårdfeldt, K., Jourdain, B., Abrahamsson, K., Granfors, A., Ahnoff, M., Dommergue, A., Méjean, G., and Jacobi, H.-W.: Antarctic winter mercury and ozone depletion events over sea ice, *Atmospheric Environment*, 129, 125-132, 2016.
- Neuman, J. A., Nowak, J. B., Huey, L. G., Burkholder, J. B., Dibb, J. E., Holloway, J. S., Liao, J., Peischl, J., Roberts, J. M., Ryerson, T. B., Scheuer, E., Stark, H., Stickel, R. E., Tanner, D. J., and Weinheimer, A.: Bromine measurements in ozone depleted air over the Arctic Ocean, *Atmos. Chem. Phys.*, 10, 6503-6514, 10.5194/acp-10-6503-2010, 2010.
- Nguyen, Q. T., Skov, H., Sørensen, L. L., Jensen, B. J., Grube, A. G., Massling, A., Glasius, M., and Nøjgaard, J. K.: Source apportionment of particles at Station Nord, North East Greenland during 2008–2010 using COPREM and PMF analysis, *Atmos. Chem. Phys.*, 13, 35-49, 10.5194/acp-13-35-2013, 2013.
- O'Driscoll, N. J., Siciliano, S. D., Lean, D. R. S., and Amyot, M.: Gross photoreduction kinetics of mercury in temperate freshwater lakes and rivers: application to a general model of DGM dynamics, *Environmental Science and Technology*, 40, 837-843, 2006.
- Palermo, C., Kay, J. E., Genthon, C., L'Ecuyer, T., Wood, N. B., and Claud, C.: How much snow falls on the Antarctic ice sheet?, *The Cryosphere*, 8, 1577-1587, 10.5194/tc-8-1577-2014, 2014.
- Parish, T. R., and Bromwich, D. H.: The surface windfield over the Antarctic ice sheets, *Nature*, 328, 51-54, 1987.



Parish, T. R., and Bromwich, D. H.: Reexamination of the near-surface airflow over the Antarctic continent and implications on atmospheric circulations at high southern latitudes, *Monthly Weather Review*, 135, 1961-1973, 2007.

Parrella, J. P., Jacob, D. J., Liang, Q., Zhang, Y., Mickley, L. J., Miller, B., Evans, M. J., Yang, X., Pyle, J. A., Theys, N., and Van Roozendaal, M.: Tropospheric bromine chemistry: implications for present and pre-industrial ozone and mercury, *Atmospheric Chemistry and Physics*, 12, 6723-6740, 2012.

Petersen, G., Munthe, J., Pleijel, K., Bloxam, R., and Kumar, A. V.: A comprehensive Eulerian modeling framework for airborne mercury species: Development and testing of the Tropospheric Chemistry module (TCM), *Atmospheric Environment*, 32, 829-843, [http://dx.doi.org/10.1016/S1352-2310\(97\)00049-6](http://dx.doi.org/10.1016/S1352-2310(97)00049-6), 1998.

Pfaffhuber, K. A., Berg, T., Hirdman, D., and Stohl, A.: Atmospheric mercury observations from Antarctica: seasonal variation and source and sink region calculations, *Atmospheric Chemistry and Physics*, 12, 3241-3251, 2012.

Pietroni, I., Argentini, S., Petenko, I., and Sozzi, R.: Measurements and parametrizations of the atmospheric boundary-layer height at Dome C, Antarctica, *Boundary-Layer Meteorology*, 143, 189-206, 2012.

Platt, U., and Janssen, C.: Observation and role of the free radicals NO₃, ClO, BrO and IO in the troposphere, *Faraday Discuss.*, 100, 175-198, 1995.

Poissant, L., and Pilote, M.: Time series analysis of atmospheric mercury in Kuujuaupik/Whapmagoostui (Québec), *J. Phys. IV France*, 107, 1079-1082, 2003.

Poulain, A. J., Lalonde, J. D., Amyot, M., Shead, J. A., Raofie, F., and Ariya, P. A.: Redox transformations of mercury in an Arctic snowpack at springtime, *Atmospheric Environment*, 38, 6763-6774, 2004.

Prestbo, E. M., and Gay, D. A.: Wet deposition of mercury in the U.S. and Canada, 1996–2005: Results and analysis of the NADP mercury deposition network (MDN), *Atmospheric Environment*, 43, 4223-4233, <http://dx.doi.org/10.1016/j.atmosenv.2009.05.028>, 2009.

Saiz-Lopez, A., Mahajan, A. S., Salmon, R. A., Bauguitte, S. J.-B., Jones, A. E., Roscoe, H. K., and Plane, J. M. C.: Boundary layer halogens in coastal antarctica, *Science*, 317, 348-351, 2007.

Sander, R., Burrows, J., and Kaleschke, L.: Carbonate precipitation in brine – a potential trigger for tropospheric ozone depletion events, *Atmos. Chem. Phys.*, 6, 4653-4658, 10.5194/acp-6-4653-2006, 2006.

Savarino, J., Kaiser, J., Morin, S., Sigman, D. M., and Thiemens, M. H.: Nitrogen and oxygen isotopic constraints on the origin of atmospheric nitrate in coastal Antarctica, *Atmospheric Chemistry and Physics*, 7, 1925-1945, 2007.

Schroeder, W. H., Anlauf, K. G., Barrie, L. A., Lu, J. Y., Steffen, A., Schneeberger, D. R., and Berg, T.: Arctic springtime depletion of mercury, *Nature*, 394, 331-332, 1998.

Selin, N. E., Jacob, D. J., Yantosca, R. M., Strode, S., Jaeglé, L., and Sunderland, E. M.: Global 3-D land-ocean-atmosphere model for mercury: present-day versus preindustrial cycles and anthropogenic enrichment factors for deposition, *Global biogeochemical cycles*, 22, doi:10.1029/2007GB003040, 2008.

Selin, N. E.: Global biogeochemical cycling of mercury: a review, *Annual Review of Environment and Resources*, 34, 43-63, 2009.



Shaw, G. E.: Evidence for a central Eurasian source area of Arctic haze in Alaska, *Nature*, 299, 815-818, 10.1038/299815a0, 1982.

Skamarock, W. C., Klemp, J. B., Dudhia, J., Gill, D. O., Barker, D. M., Wang, W., and Powers, J. G.: A description of the advanced research WRF version 2. NCAR/TN-468+STR. NCAR Technical Note. Boulder, CO, USA, 2007.

Skov, H., Christensen, J. H., Goodsite, M. E., Heidam, N. Z., Jensen, B., Wählin, P., and Geernaert, G.: Fate of Elemental Mercury in the Arctic during Atmospheric Mercury Depletion Episodes and the Load of Atmospheric Mercury to the Arctic, *Environmental Science & Technology*, 38, 2373-2382, 10.1021/es030080h, 2004.

Slemr, F., Angot, H., Dommergue, A., Magand, O., Barret, M., Weigelt, A., Ebinghaus, R., Brunke, E.-G., Pfaffhuber, K. A., Edwards, G., Howard, D., Powell, J., Keywood, M., and Wang, F.: Comparison of mercury concentrations measured at several sites in the Southern Hemisphere, *Atmospheric Chemistry and Physics*, 15, 3125-3133, 2015.

Soerensen, A. L., Sunderland, E. M., Holmes, C. D., Jacob, D. J., Yantosca, R. M., Skov, H., Christensen, J. H., Strode, S. A., and Mason, R. P.: An improved global model for air-sea exchange of mercury: high concentrations over the north atlantic, *Environmental Science and Technology*, 44, 8574-8580, 2010.

Soerensen, A. L., Jacob, D. J., Schartup, A. T., Fisher, J. A., Lehnerr, I., St. Louis, V. L., Heimbürger, L.-E., Sonke, J. E., Krabbenhoft, D. P., and Sunderland, E. M.: A mass budget for mercury and methylmercury in the Arctic Ocean, *Global biogeochemical cycles*, 30, 10.1002/2015GB005280, 2016.

Sommar, J., Gårdfeldt, K., Strömberg, D., and Feng, X.: A kinetic study of the gas-phase reactions between the hydroxyl radical and atomic mercury, *Atmospheric Environment*, 35, 3049-3054, 2001.

Sommar, J., Wängberg, I., Berg, T., Gårdfeldt, K., Munthe, J., Richter, A., Urba, A., Wittrock, F., and Schroeder, W. H.: Circumpolar transport and air-surface exchange of atmospheric mercury at Ny-Alesund (79°N), Svalbard, spring 2002, *Atmos. Chem. Phys.*, 7, 151-166, 10.5194/acp-7-151-2007, 2007.

Song, S., Selin, N. E., Soerensen, A. L., Angot, H., Artz, R., Brooks, S., Brunke, E.-G., Conley, G., Dommergue, A., Ebinghaus, R., Holsen, T. M., Jaffe, D. A., Kang, D., Kelley, P., Luke, W. T., Magand, O., Marumoto, K., Pfaffhuber, K. A., Ren, X., Sheu, G.-R., Slemr, F., Warneke, T., Weigelt, A., Weiss-Penzias, P., Wip, D. C., and Zhang, Q.: Top-down constraints on atmospheric mercury emissions and implications for global biogeochemical cycling, *Atmospheric Chemistry and Physics*, 15, 7103-7125, 2015.

Sprenn, G., Kaleschke, L., and Heygster, G.: Sea ice remote sensing using AMSR-E 89 GHz channels, *Journal of geophysical research*, 113, <http://dx.doi.org/10.1029/2005JC003384>, 2008.

Sprovieri, F., Pirrone, N., Hedgecock, I. M., Landis, M. S., and Stevens, R. K.: Intensive atmospheric mercury measurements at Terra Nova Bay in antarctica during November and December 2000, *Journal of geophysical research*, 107, 4722, 2002.

Sprovieri, F., Pirrone, N., Landis, M. S., and Stevens, R. K.: Oxidation of Gaseous Elemental Mercury to Gaseous Divalent Mercury during 2003 Polar Sunrise at Ny-Alesund, *Environmental Science & Technology*, 39, 9156-9165, 10.1021/es050965o, 2005a.



Sprovieri, F., Pirrone, N., Landis, M. S., and Stevens, R. K.: Atmospheric mercury behavior at different altitudes at Ny Alesund during Spring 2003, *Atmospheric Environment*, 39, 7646-7656, <http://dx.doi.org/10.1016/j.atmosenv.2005.08.001>, 2005b.

Sprovieri, F., Pirrone, N., Ebinghaus, R., Kock, H. H., and Dommergue, A.: A review of worldwide atmospheric mercury measurements, *Atmospheric Chemistry and Physics*, 10, 8245-8265, 2010.

Sprovieri, F., Pirrone, N., Bencardino, M., D'Amore, F., Cinnirella, S., Esposito, G., Landis, M., Ebinghaus, R., Weigelt, A., Brunke, E.-G., Martin, L., Munthe, J., Wängberg, I., Artaxo, P., Morais, F., Cairns, W., Barbante, C., Diéguez, M., Garcia, P. E., Dommergue, A., Angot, H., Magand, O., Skov, H., Horvat, M., Kotnik, J., Read, K. A., Neves, M., Gawlik, B. M., Sena, F., Mashyanov, N., Wip, D. C., Feng, S. X., Hui, Z., Ramachandran, R., Cossa, D., Knoery, J., and Maruschak, N.: Atmospheric mercury concentrations observed at ground-based monitoring sites globally distributed in the framework of the GMOS network, this issue-a.

Sprovieri, F., Pirrone, N., Bencardino, M., D'Amore, F., Wangberg, I., Munthe, J., Ebinghaus, R., Weigelt, A., Brunke, E.-G., Martin, A. P., Dommergue, A., Angot, H., Magand, O., Barbante, C., Cairns, W., Gawlik, B. M., Sena, F., Vardè, M., Horvat, M., Kotnik, J., Dieguez, M., Feng, S. X., Hui, Z., and Mashyanov, N.: Five-year records of total mercury deposition fluxes at GMOS sites in the Northern and Southern Hemispheres, this issue-b.

Steen, A. O., Berg, T., Dastoor, A. P., Durnford, D. A., Hole, L. R., and Pfaffhuber, K. A.: Dynamic exchange of gaseous elemental mercury during polar night and day, *Atmospheric Environment*, 43, 5604-5610, <http://dx.doi.org/10.1016/j.atmosenv.2009.07.069>, 2009.

Steen, A. O., Berg, T., Dastoor, A. P., Durnford, D. A., Engelsen, O., Hole, L. R., and Pfaffhuber, K. A.: Natural and anthropogenic atmospheric mercury in the European Arctic: a fractionation study, *Atmos. Chem. Phys.*, 11, 6273-6284, 10.5194/acp-11-6273-2011, 2011.

Steffen, A., Schroeder, W., Bottenheim, J., Narayan, J., and Fuentes, J. D.: Atmospheric mercury concentrations: measurements and profiles near snow and ice surfaces in the Canadian Arctic during Alert 2000, *Atmospheric Environment*, 36, 2653-2661, 2002.

Steffen, A., Schroeder, W. H., Edwards, G., and Banic, C.: Mercury throughout polar sunrise 2002, *J. Phys. IV France*, 107, 1267-1270, 2003.

Steffen, A., Schroeder, W., Macdonald, R., Poissant, L., and Konoplev, A.: Mercury in the Arctic atmosphere: An analysis of eight years of measurements of GEM at Alert (Canada) and a comparison with observations at Amderma (Russia) and Kuujuarapik (Canada), *Science of The Total Environment*, 342, 185-198, <http://dx.doi.org/10.1016/j.scitotenv.2004.12.048>, 2005.

Steffen, A., Douglas, T., Amyot, M., Ariya, P. A., Aspino, K., Berg, T., Bottenheim, J., Brooks, S., Cobbett, F., Dastoor, A., Dommergue, A., Ebinghaus, R., Ferrari, C., Gardfeldt, K., Goodsite, M. E., Lean, D., Poulain, A. J., Scherz, C., Skov, H., Sommar, J., and Temme, C.: A synthesis of atmospheric mercury depletion event chemistry in the atmosphere and snow, *Atmospheric Chemistry and Physics*, 8, 1445-1482, 2008.

Steffen, A., Scherz, T., Oslon, M., Gay, D. A., and Blanchard, P.: A comparison of data quality control protocols for atmospheric mercury speciation measurements, *Journal of Environmental Monitoring*, 14, 752-765, doi: 10.1039/c2em10735j, 2012.



Steffen, A., Bottenheim, J., Cole, A., Ebinghaus, R., Lawson, G., and Leitch, W. R.: Atmospheric mercury speciation and mercury in snow over time at Alert, Canada, *Atmospheric Chemistry and Physics*, 14, 2219-2231, 2014.

Steffen, A., Lehnher, I., Cole, A., Ariya, P., Dastoor, A., Durnford, D., Kirk, J., and Pilote, M.: Atmospheric mercury in the Canadian Arctic. Part I: A review of recent field measurements, *Science of The Total Environment*, 509-510, 3-15, <http://dx.doi.org/10.1016/j.scitotenv.2014.10.109>, 2015.

Stephens, G. L., Vane, D. G., Tanelli, S., Eastwood, I., Durden, S., Rokey, M., Reinke, D., Partain, P., Mace, G. G., Austin, R., L'Ecuyer, T., Haynes, J., Lebsock, M., Suzuki, K., Waliser, D., Wu, D., Kay, J., Gettelman, A., Wang, Z., and Marchand, R.: CloudSat mission: performance and early science after the first year of operation, *Journal of geophysical research*, 113, <http://dx.doi.org/10.1029/2008JD009982>, 2008.

Subir, M., Ariya, P. A., and Dastoor, A.: A review of uncertainties in atmospheric modeling of mercury chemistry I. Uncertainties in existing kinetic parameters - fundamental limitations and the importance of heterogeneous chemistry, *Atmospheric Environment*, 45, 5664-5675, 2011.

Subir, M., Ariya, P. A., and Dastoor, A.: A review of the sources of uncertainties in atmospheric mercury modeling II. Mercury surface and heterogeneous chemistry - a missing link, *Atmospheric Environment*, 46, 1-10, 2012.

Tarasick, D. W., and Bottenheim, J. W.: Surface ozone depletion episodes in the Arctic and Antarctic from historical ozonesonde records, *Atmos. Chem. Phys.*, 2, 197-205, 10.5194/acp-2-197-2002, 2002.

Tekran: Tekran 2537 mercury monitor detection limit. Summary of known estimates, Tekran Instruments Corp., Toronto, ON, Canada., 2011.

Temme, C., Einax, J. W., Ebinghaus, R., and Schroeder, W. H.: Measurements of atmospheric mercury species at a coastal site in the antarctic and over the atlantic ocean during polar summer, *Environmental Science and Technology*, 37, 22-31, 2003.

Theys, N., Van Roozendael, M., Hendrick, F., Yang, X., De Smedt, I., Richter, A., Begoin, M., Errera, Q., Johnston, P. V., Kreher, K., and De Mazière, M.: Global observations of tropospheric BrO columns using GOME-2 satellite data, *Atmospheric Chemistry and Physics*, 11, 1791-1811, 2011.

Tossell, J. A.: Calculation of the energetics for oxidation of gas-phase elemental Hg by Br and BrO, *The Journal of physical chemistry A*, 107, 7804-7808, 2003.

Toyota, K., Dastoor, A., and Ryzhkov, A.: Air-snowpack exchange of bromine, ozone and mercury in the springtime Arctic simulated by the 1-D model PHANTAS - Part 2: mercury and its speciation, *Atmospheric Chemistry and Physics*, 14, 4135-4167, 2014.

Travnikov, O., and Ilyin, I.: The EMEP/MSC-E Mercury Modelling System, in: *Mercury Fate and Transport in the Global Atmosphere: Emissions, Measurements, and Models*, edited by: Pirrone, N., and Mason, R. P., Springer, 571-587, 2009.

Travnikov, O., Dastoor, A., De Simone, F., Hedgecock, I. M., Pirrone, N., Ryzhkov, A., Selin, N. E., Song, S., and Yang, X.: Multi-model study of mercury dispersion in the atmosphere: Atmospheric processes and model evaluation, in preparation.

UNEP: Text of the Minamata Convention on Mercury for adoption by the Conference of Plenipotentiaries. [unep.org](http://www.unep.org/hazardoussubstances/Portals/9/Mercury/Documents/dipcon/CONF_3_M). July 31, Available at: http://www.unep.org/hazardoussubstances/Portals/9/Mercury/Documents/dipcon/CONF_3_M



[inamata%20Convention%20on%20Mercury_final%2026%2008_e.pdf](#), last access: 27 March 2016, 2013a.

UNEP: Global Mercury Assessment 2013: Sources, Emissions, Releases and Environmental Transport. UNEP Chemicals Branch, Geneva, Switzerland, 44 pp., 2013b.

UNEP: Global mercury modelling: update of modelling results in the global mercury assessment 2013, 2015.

Wang, J., Zhang, L., and Xie, Z.: Total gaseous mercury along a transect from coastal to central Antarctic: Spatial and diurnal variations, *Journal of Hazardous Materials*, <http://dx.doi.org/10.1016/j.jhazmat.2016.05.068>, 2016.

Wang, P.: Atmospheric mercury speciation and aerosol properties at Ny-Alesund, Department of Chemistry, Norwegian University of Science and Technology, 130 pp., 2015.

Yang, X., Cox, R. A., Warwick, N. J., Pyle, J. A., Carver, G. D., O'Connor, F. M., and Savage, N. H.: Tropospheric bromine chemistry and its impacts on ozone: A model study, *Journal of geophysical research*, 110, 10.1029/2005JD006244, 2005.

Yu, J., Xie, Z., Kang, H., Li, Z., Sun, C., Bian, L., and Zhang, P.: High variability of atmospheric mercury in the summertime boundary layer through the central Arctic Ocean, *Scientific Reports*, 4, 6091, 10.1038/srep06091

<http://www.nature.com/articles/srep06091#supplementary-information>, 2014.

Zambrano-Bigiarini, M.: hydroGOF: Goodness-of-fit functions for comparison of simulated and observed hydrological time series. R package version 0.3-8. <http://CRAN.R-project.org/package=hydroGOF>, 2014.

Zatko, M., Geng, L., Alexander, B., Sofen, E., and Klein, K.: The impact of snow nitrate photolysis on boundary layer chemistry and the recycling and redistribution of reactive nitrogen across Antarctica and Greenland in a global chemical transport model, *Atmos. Chem. Phys.*, 16, 2819-2842, 10.5194/acp-16-2819-2016, 2016.

Zatko, M. C., Grenfell, T. C., Alexander, B., Doherty, S. J., Thomas, J. L., and Yang, X.: The influence of snow grain size and impurities on the vertical profiles of actinic flux and associated NO_x emissions on the Antarctic and Greenland ice sheets, *Atmospheric Chemistry and Physics*, 13, 3547-3567, 2013.

Zhu, W., Lin, C. J., Wang, X., Sommar, J., Fu, X., and Feng, X.: Global observations and modeling of atmosphere-surface exchange of elemental mercury: a critical review, *Atmos. Chem. Phys.*, 16, 4451-4480, 10.5194/acp-16-4451-2016, 2016.



	Code	Elevation (m a.s.l.)	Analyte	Instrumentation	Flow rate (L/min)	Resolution	Filter at the inlet	Sampling line
Arctic	ALT	195	Hg(0)	Tekran 2537A	1.0	5 min		
			Hg(p), RGM	Tekran 2537A/1130/1135	10.0	2 h	speciation unit	heated
	SND	30	Hg(0)	Tekran 2537A	1.5	5 min	sodalime	heated
	NYA	474	Hg(0)	Tekran 2537A	1.5	5 min	2 µm PTFE and sodalime	heated
	AND	10	Hg(0)	Tekran 2537A	1.5	5 min	2 µm PTFE and sodalime	heated
Antarctica	TR	1275	Hg(0)	Tekran 2537A	1.5	5 min	2 µm PTFE filter	unheated
	DC	3220	Hg(0)	Tekran 2537A	0.8	5-15 min	0.45 µm PTFE filter	unheated
	DDU	43	Hg(0)	Tekran 2537B	1.0	10-15 min	0.20 µm PTFE filter	unheated
	ANT	20	Hg(0)	Tekran 2537A	1.0	5 min		
			Hg(p), RGM	Tekran 2537A/1130/1135	10.0	2 h	speciation unit	heated
	OSO	15	Hg(0)	Tekran 2537A	1.0	5 min	0.45 µm PTFE filter	unheated

Table 1: Summary of the instrumentation used at the various Polar sites to measure atmospheric mercury species.



Station	2011			2012			2013			2014			2015								
	n	mean	SD	n	mean	SD	n	mean	SD	n	mean	SD	n	mean	SD						
Arctic	ALT	8040	1.39	1.35	0.45	8447	1.21	1.21	0.35	8048	1.31	1.39	0.46	8358	1.45	1.45	0.33	na	na	na	na
	SND	4712	1.26	1.34	0.32	7932	1.44	1.44	0.26	6605	1.57	1.49	0.44	4991	1.36	1.36	0.35	1059	1.11	1.11	0.32
	NYA	8173	1.51	1.59	0.31	8181	1.51	1.54	0.21	6980	1.47	1.52	0.30	6730	1.48	1.57	0.33	8342	1.49	1.49	0.21
	AND	7444	1.61	1.61	0.15	8428	1.61	1.61	0.13	7862	1.53	1.56	0.15	8146	1.50	1.51	0.16	7146	1.50	1.50	0.10
Antarctica	TR	5978	0.95	0.99	0.20	7808	0.98	0.97	0.15	8197	0.90	0.93	0.15	7421	0.95	1.00	0.21	3670	0.94	0.93	0.31
	DC	na	na	na	na	3761	0.76	0.70	0.24	2900	0.84	0.87	0.27	na	na	na	na	8383	1.06	1.12	0.41
	DDU	na	na	na	na	5949	0.91	0.92	0.20	5121	0.85	0.85	0.19	1958	0.85	0.82	0.38	3114	0.86	0.87	0.19

Table 2: Annually-based statistics (number of hourly-averaged data (n), mean, median, standard deviation (SD)) of Hg(0) concentrations (in ng m⁻³) at ground-based Polar sites over the 2011-2015 period. Note that 2013 data at DC refer to concentrations recorded at 210 cm above the snowpack. The 2015 data coverage is May to June at SND and January to May at DDU (see Table 3). na: not available due to QA/QC invalidation, instrument failure, or because the QA/QC validation is currently in progress (2015 data).



	GLEMOS			GEOS-Chem			GEM-MACH-Hg			ECHMERIT		
	NSE	RMSE	PBIAS	NSE	RMSE	PBIAS	NSE	RMSE	PBIAS	NSE	RMSE	PBIAS
ALT	0.12	0.29	4.9	0.32	0.25	1.3	0.49	0.22	4.1	-0.27	0.34	-10.0
SND	-0.83	0.29	-12.0	-0.85	0.29	-13.7	-0.17	0.23	-9.0	-2.85	0.42	-22.7
NYA	0.00	0.11	-6.3	-1.82	0.18	-9.7	-0.40	0.13	-4.4	-4.16	0.25	-15.5
AND	-2.76	0.20	-8.3	-2.50	0.19	-12.2	-0.26	0.12	-4.1	-6.24	0.28	-16.7
TR	-1.83	0.13	14.0	-4.76	0.19	3.0	-2.98	0.16	10.2	-2.50	0.15	-11.8
DC	-0.28	0.19	16.2	-1.07	0.25	7.5	-1.08	0.25	16.3	-0.32	0.20	-6.6
DDU	-6.10	0.24	25.4	-8.15	0.27	16.9	-4.87	0.22	16.7	-0.85	0.12	-5.1

Table 4: Goodness-of-fit statistics between monthly-averaged (year 2013) modeled and observed Hg(0) data at all ground-based sites: Nash-Sutcliffe efficiency (NSE, quantity without unit), root mean square error (RMSE, in ng/m³), and percent bias (PBIAS, in %).



	GEOS-Chem				GEM-MACH-Hg			
	2011	2012	2013	2014	2011	2012	2013	2014
<i>Summer</i>								
ALT	-23.9	-1.9	-15.4	-17.1	-12.3	11.1	-9.2	-10.0
SND	34.3	-3.8	-22.0	4.6	11.6	1.4	-17.5	3.4
NYA	-8.9	-7.3	-14.7	-15.6	-5.9	-4.4	-0.2	-1.0
AND	-13.2	-10.4	-11.9	-14.1	-7.2	-6.8	3.2	3.0
TR	-1.1	-14.0	-8.9	-5.6	4.0	-1.9	6.3	23.6
DC	na	1.7	15.6	na	na	8.7	35.6	na
DDU	na	0.1	0.0	-8.3	na	-3.4	-1.7	8.4
<i>Fall</i>								
ALT	9.4	11.7	-9.8	-9.5	13.4	14.7	-3.6	-3.0
SND	-3.3	-1.5	-9.1	23.4	2.7	-0.5	-5.0	26.8
NYA	-11.1	-7.9	-14.4	-12.0	-9.3	-8.4	-9.7	-8.5
AND	-12.6	-11.1	-15	-12.1	-13.4	-12.5	-13.9	-6.5
TR	-13.1	-12.0	-10.9	-24.6	-7.8	-1.4	-2.9	-11.6
DC	na	-31.5	-22.6	na	na	-18.6	-43.4	na
DDU	na	-9.6	1.1	-19.9	na	-3.2	2.1	-4.4
<i>Winter</i>								
ALT	11.8	18.5	11.7	3.3	12.8	19.2	16.2	8.0
SND	5.5	5.5	4.2	11.6	5.1	4.8	5.5	15.3
NYA	4.1	0.1	-3.0	-4.0	1.3	-1.4	-1.4	-1.5
AND	-7.6	-9.0	-8.0	-7.6	-10.1	-11.1	-7.2	-6.7
TR	25.3	29.8	29.6	14.1	5.8	9.2	11.3	2.8
DC	na	79.9	39.3	na	na	48.4	17.8	na
DDU	na	38.5	50.4	49.4	na	15.4	26.9	40.4
<i>Spring</i>								
ALT	3.2	27.4	29.7	-21.8	-23.0	9.3	11.8	-24.0
SND	12.3	-11.6	-25.5	-33.3	4.2	-27.7	-23.0	-18.8
NYA	-5.8	-5.3	-9.7	-17.8	-23.8	-17.0	-21.5	-20.4
AND	-11.5	-13.8	-12.4	-16.7	-9.3	-16.0	-5.5	-7.6
TR	na	-9.0	13.0	-7.7	na	7.5	36.5	18.1
DC	na	32.6	22.9	na	na	48.8	34.5	na
DDU	na	3.2	73.6	na	na	31.9	62.8	na

Table 5: Percent bias (in %) between hourly-averaged modeled and observed Hg(0) data at all ground-based sites. Summer refers to Jun - Aug (Nov - Feb), fall to Sep - Nov (Mar - Apr), winter to Dec - Feb (May - Aug), and spring to Mar - May (Sep - Oct) at Arctic (Antarctic) sites. na: not available due to QA/QC invalidation, or instrument failure.

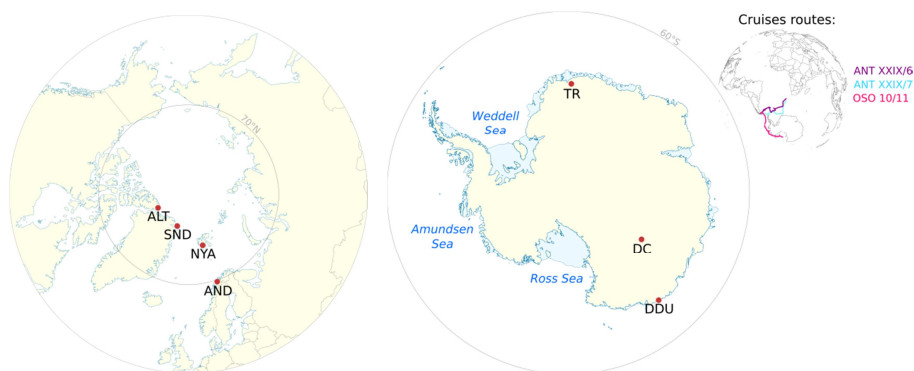


Figure 1: Location of the sites whose data are reported in this paper: Alert (ALT), Villum Research Station at Station Nord (SND), Zeppelin station at Ny-Ålesund (NYA), Andøya (AND), Troll (TR), Concordia Station at Dome C (DC), and Dumont d'Urville (DDU). Additionally, two cruises were performed in Antarctica: ANT XXIX/6-7 (denoted ANT in the paper) over the Weddell Sea onboard icebreaker Polarstern, and OSO 10/11 (denoted OSO in the paper) over Ross and Amundsen Seas onboard icebreaker Oden.

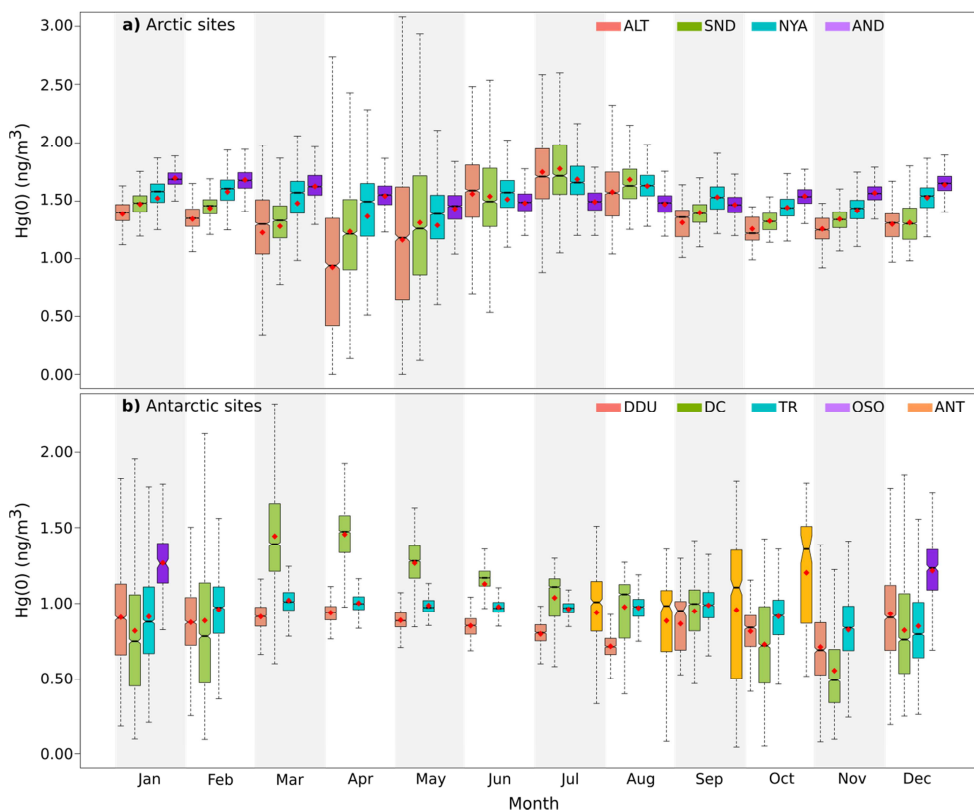


Figure 2: Box and whisker plots presenting the monthly Hg(0) concentration distribution at **a)** Arctic sites: ALT (red), SND (green), NYA (turquoise), AND (purple), and **b)** Antarctic sites: DDU (red), DC (green), TR (turquoise), during the OSO (purple) and ANT (orange) cruises. ♦: mean, bottom and top of the box: first and third quartiles, band inside the box: median, ends of the whiskers: lowest (highest) datum still within the 1.5 interquartile range of the lowest (upper) quartile. Outliers are not represented.

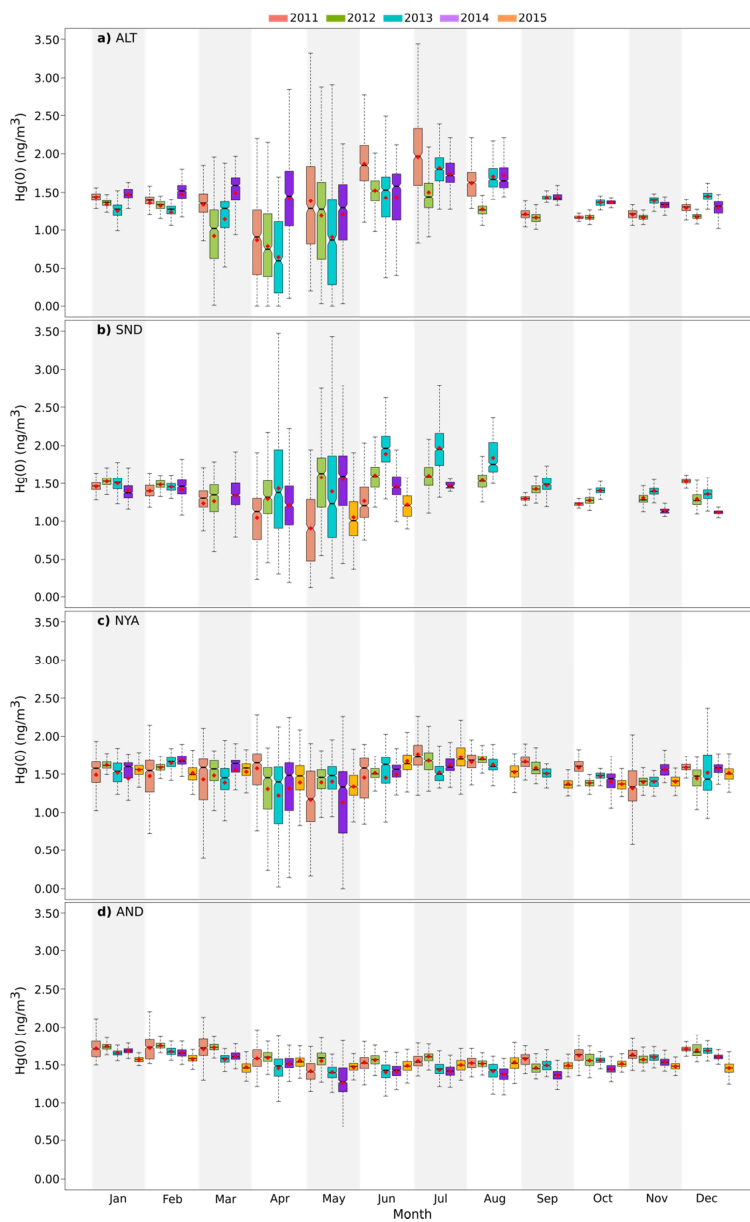


Figure 3: Box and whisker plots presenting the monthly Hg(0) concentration distribution at Arctic sites **a)** ALT, **b)** SND, **c)** NYA, and **d)** AND in 2011 (pink), 2012 (green), 2013 (turquoise), 2014 (purple), and 2015 (orange). ♦: mean, bottom and top of the box: first and third quartiles, band inside the box: median, ends of the whiskers: lowest (highest) datum still within the 1.5 interquartile range of the lowest (upper) quartile. Outliers are not represented.

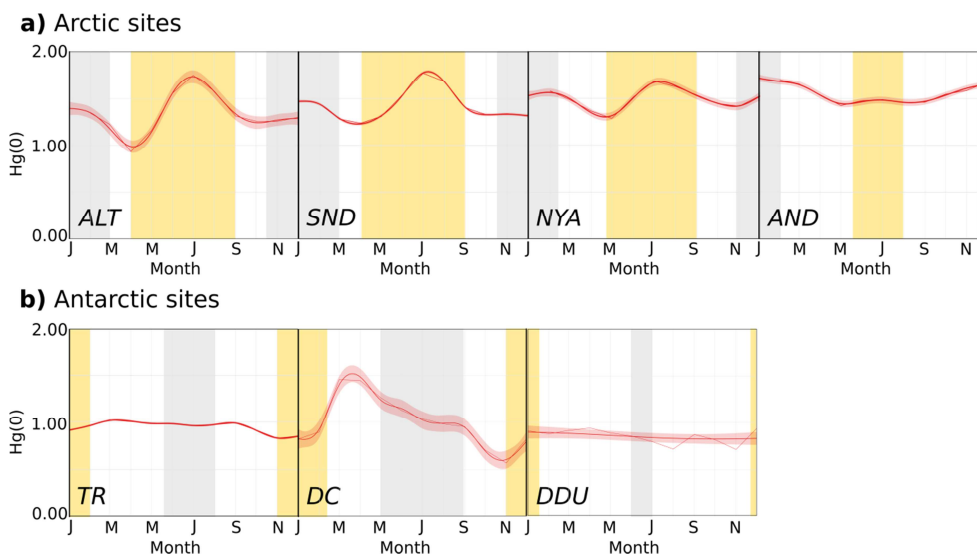


Figure 4: Seasonal variation (monthly mean along with the 95% confidence interval for the mean) of Hg(0) concentrations (in ng m⁻³) at **a)** Arctic and **b)** Antarctic ground-based sites. Periods highlighted in yellow refer to 24-h sunlight and periods highlighted in grey to 24-h darkness. Summer refers to June – August (November – February), fall to September – November (March – April), winter to December – February (May – August), and spring to March – May (September – October) at Arctic (Antarctic) sites.

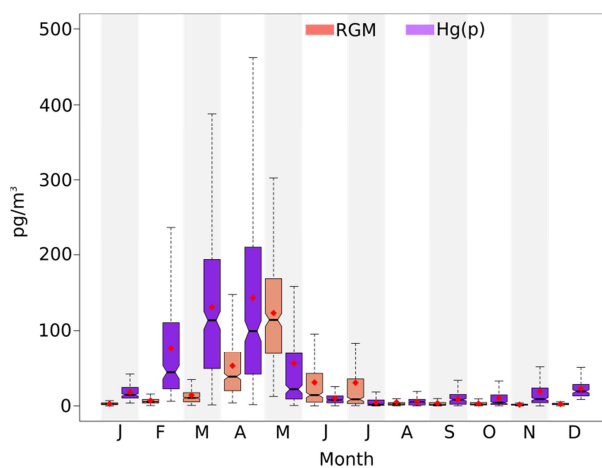


Figure 5: Box and whisker plots presenting the monthly RGM (in red) and Hg(p) (in violet) concentration distribution (in pg m^{-3}) at ALT over the 2011-2014 period. ♦: mean, bottom and top of the box: first and third quartiles, band inside the box: median, ends of the whiskers: lowest (highest) datum still within the 1.5 interquartile range of the lowest (upper) quartile. Outliers are not represented.

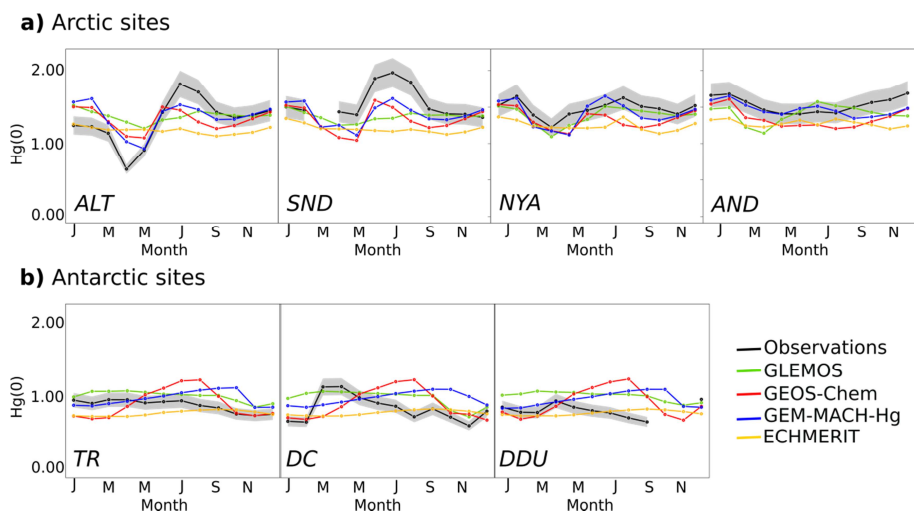


Figure 6: Year 2013 monthly-averaged Hg(0) concentrations (in ng m⁻³) at **a)** Arctic and **b)** Antarctic ground-based sites: observations (in black) and concentrations according to the four global models (GLEMOS in green, GEOS-Chem in blue, GEM-MACH-Hg in red, ECHMERIT in yellow). The gray shaded regions indicate a 10 % uncertainty for observations.

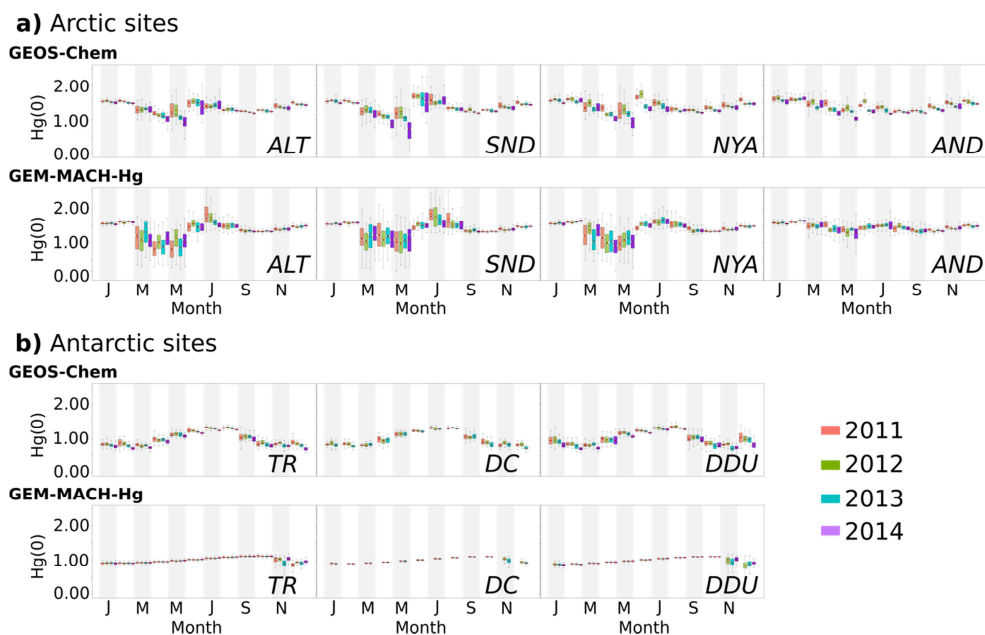


Figure 7: Box and whisker plots presenting the monthly $\text{Hg}(0)$ concentration distribution at **a)** Arctic and **b)** Antarctic ground-based sites as simulated by GEOS-Chem and GEM-MACH-Hg in 2011 (pink), 2012 (green), 2013 (turquoise), and 2014 (purple). \blacklozenge : mean, bottom and top of the box: first and third quartiles, band inside the box: median, ends of the whiskers: lowest (highest) datum still within the 1.5 interquartile range of the lowest (upper) quartile. Outliers are not represented.

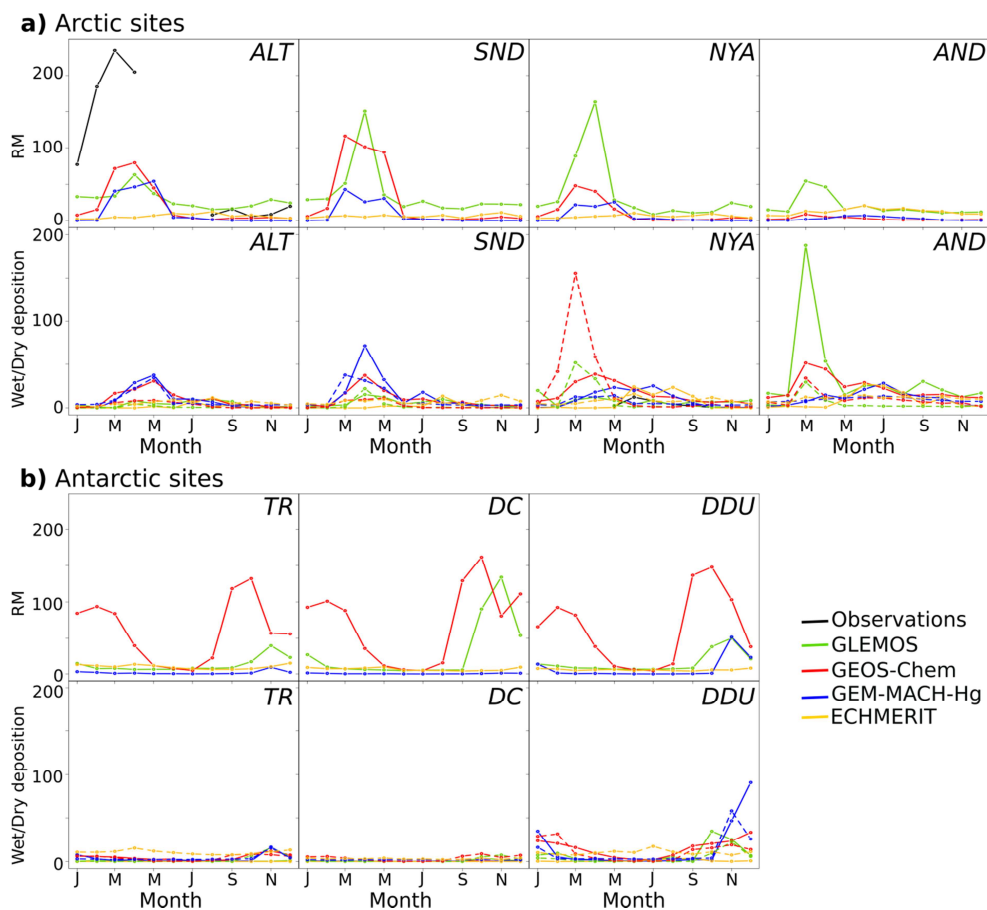


Figure 8: Year 2013 monthly-averaged mean reactive mercury (RM) concentrations (in pg m^{-3}) along with mean wet (solid line) and dry (dashed line) deposition (in $\text{ng m}^{-2} \text{day}^{-1}$) at **a)** Arctic and **b)** Antarctic ground-based sites: observations (in black) and concentrations according to the four global models (GLEMOS in green, GEOS-Chem in red, GEM-MACH-Hg in blue, ECHMERIT in yellow). Note that RM (wet deposition) observations are available at ALT (NYA) only.

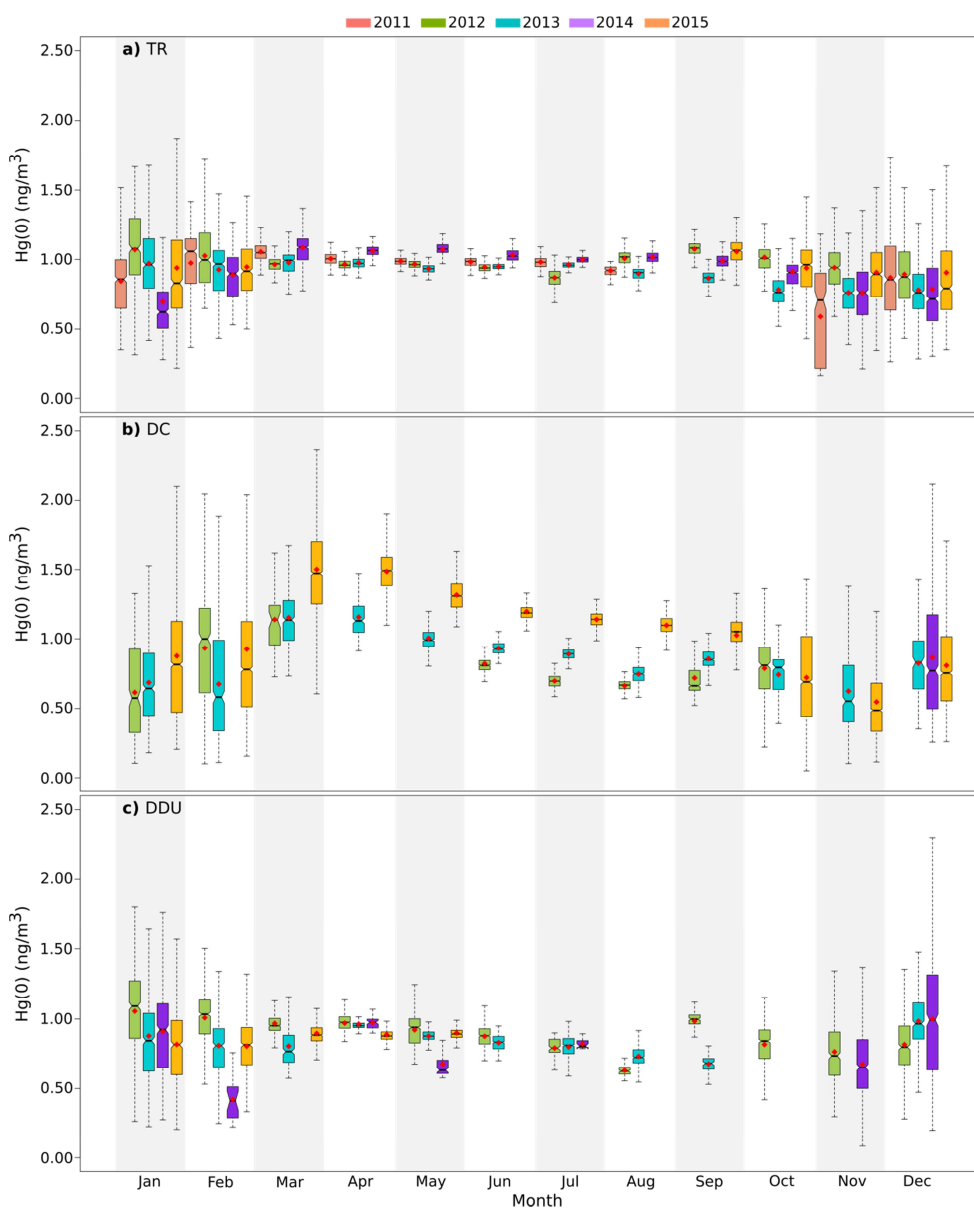


Figure 9: Box and whisker plots presenting the monthly Hg(0) concentration distribution at ground-based Antarctic sites **a)** TR, **b)** DC, and **c)** DDU in 2011 (pink), 2012 (green), 2013 (turquoise), 2014 (purple), and 2015 (orange). ♦: mean, bottom and top of the box: first and third quartiles, band inside the box: median, ends of the whiskers: lowest (highest) datum still within the 1.5 interquartile range of the lowest (upper) quartile. Outliers are not represented.